

Article

## Exploration of Fragment Binding Poses Leading to Efficient Discovery of Highly Potent and Orally Effective Inhibitors of FABP4 for Anti-inflammation

Haixia Su, Yi Zou, Guofeng Chen, Huixia Dou, Hang Xie, Xiaojing Yuan, Xianglei Zhang, Naixia Zhang, Minjun Li, and Yechun Xu

*J. Med. Chem.*, **Just Accepted Manuscript** • DOI: 10.1021/acs.jmedchem.9b02107 • Publication Date (Web): 23 Mar 2020

Downloaded from [pubs.acs.org](https://pubs.acs.org) on March 23, 2020

### Just Accepted

“Just Accepted” manuscripts have been peer-reviewed and accepted for publication. They are posted online prior to technical editing, formatting for publication and author proofing. The American Chemical Society provides “Just Accepted” as a service to the research community to expedite the dissemination of scientific material as soon as possible after acceptance. “Just Accepted” manuscripts appear in full in PDF format accompanied by an HTML abstract. “Just Accepted” manuscripts have been fully peer reviewed, but should not be considered the official version of record. They are citable by the Digital Object Identifier (DOI®). “Just Accepted” is an optional service offered to authors. Therefore, the “Just Accepted” Web site may not include all articles that will be published in the journal. After a manuscript is technically edited and formatted, it will be removed from the “Just Accepted” Web site and published as an ASAP article. Note that technical editing may introduce minor changes to the manuscript text and/or graphics which could affect content, and all legal disclaimers and ethical guidelines that apply to the journal pertain. ACS cannot be held responsible for errors or consequences arising from the use of information contained in these “Just Accepted” manuscripts.

1  
2  
3  
4 **Exploration of Fragment Binding Poses Leading to Efficient Discovery**  
5  
6 **of Highly Potent and Orally Effective Inhibitors of FABP4 for Anti-**  
7  
8 **inflammation**  
9  
10

11  
12  
13  
14 Haixia Su<sup>Δ,§,#</sup>, Yi Zou<sup>Δ,#</sup>, Guofeng Chen<sup>Δ,§,#</sup>, Huixia Dou<sup>Δ,#</sup>, Hang Xie<sup>Δ</sup>, Xiaojing  
15  
16 Yuan<sup>Δ</sup>, Xianglei Zhang<sup>Δ,§</sup>, Naixia Zhang<sup>Δ,§</sup>, Minjun Li<sup>‡</sup>, Yechun Xu<sup>Δ,§,\*</sup>  
17  
18

19  
20 <sup>Δ</sup>CAS Key Laboratory of Receptor Research, Drug Discovery and Design Center,  
21  
22 Department of Analytical Chemistry, Shanghai Institute of Materia Medica,  
23  
24 Chinese Academy of Sciences, Shanghai 201203, China  
25

26  
27 <sup>§</sup>University of Chinese Academy of Sciences, Beijing 100049  
28  
29

30 <sup>‡</sup>Shanghai Synchrotron Radiation Facility, Shanghai Advanced Research Institute,  
31  
32 Chinese Academy of Sciences, Shanghai 201210, China  
33  
34  
35  
36  
37  
38  
39  
40  
41  
42  
43  
44  
45  
46  
47  
48  
49  
50  
51  
52  
53  
54  
55  
56  
57  
58  
59  
60

## ABSTRACT

Fatty-acid binding protein 4 (FABP4) is a promising therapeutic target for immunometabolic diseases, while its potential for systemic inflammatory response syndrome treatment has not been explored. Here, a series of 2-(phenylamino)benzoic acids as novel and potent FABP4 inhibitors are rationally designed based on an interesting fragment which adopts multiple binding poses within FABP4. A fusion of these binding poses leads to design of compound **3** with a ~460-fold improvement in binding affinity compared to the initial fragment. A subsequent structure-aided optimization upon **3** results in a promising lead (**17**) with the highest binding affinity among all the inhibitors, exerting a significant anti-inflammatory effect in cells and effectively attenuating a systemic inflammatory damage in mice. Our work therefore presents a good example of lead compounds discovery derived from the multiple binding poses of a fragment and provides a candidate for development of drugs against inflammation-related diseases.

## ■ INTRODUCTION

Fatty-acid binding proteins (FABPs) are a class of lipid chaperones involved in regulation of the uptake and intracellular transport of fatty acids (FAs). So far, 10 different FABPs with tissue-specific expression have been identified.<sup>1</sup> Among them, FABP4 is predominantly expressed in mature adipocytes and macrophages, acting as an important regulator in inflammatory-related signaling pathways.<sup>2,3</sup> In macrophages, FABP4 aggravates the lipopolysaccharide (LPS)-induced inflammatory response by the formation of a positive feedback loop with c-Jun N-terminal Kinase (JNK) and activate protein 1 (AP-1).<sup>4</sup> In addition, FABP4 can disturb the eicosanoid homostasis by regulating the activity of cyclooxygenase 2 (COX2) and the stability of leukotriene A4 (LTA4), ultimately exerting an impact on macrophages functions and inflammatory response.<sup>5,6</sup> It has been reported that FABP4-deficient macrophages exhibit a dramatic decrease in production of inflammatory cytokines including monocyte chemo-attractant

1  
2  
3  
4 protein 1 (MCP-1), interleukin 6 (IL-6), tumor necrosis factor  $\alpha$  (TNF- $\alpha$ ), and  
5 interleukin 1 $\beta$  (IL-1 $\beta$ ).<sup>7,8</sup> In adipocytes, a fat-specific deletion of FABP4 also decreases  
6 the expression of inflammatory cytokines.<sup>9</sup> FABP4 inhibition or knockout in mice has  
7 acquired therapeutic benefits for inflammation-associated diseases, such as  
8 atherosclerosis,<sup>8,10,11</sup> renal interstitial fibrosis,<sup>12</sup> non-alcoholic steatohepatitis,<sup>13,14</sup> and  
9 acute lung injury.<sup>15</sup> Accordingly, FABP4 inhibitors provide the therapeutic potential  
10 for these diseases.<sup>16</sup>

11  
12  
13  
14  
15  
16  
17  
18 It is noteworthy that FABP3-deficient mice suffered from a regional cardiac  
19 hypertrophy and stress-intolerability.<sup>17</sup> The selectivity of inhibitors for FABP4 over  
20 FABP3 has to be considered in order to avoid the potential cardiac toxicity. In contrast,  
21 FABP4/FABP5 double-knockout mice displayed a more significant protection from  
22 insulin resistance, type 2 diabetes, and atherosclerosis compared to FABP4 or FABP5  
23 single-knockout.<sup>18</sup> FABP4/FABP5 dual inhibitors are thus expected to have great utility  
24 in treating these diseases. Recently, Li *et al.* reported that it is FABP4 rather than  
25 FABP5 that promoted the growth and metastasis of breast cancer.<sup>19</sup> Accordingly,  
26 FABP4 selective inhibitors may afford a better choice for the treatment of cancer. In  
27 terms of anti-inflammation, there is no evidence to show that FABP4/FABP5 dual  
28 inhibitors would have better efficacy than the FABP4 selective inhibitors do.

29  
30  
31  
32  
33  
34  
35  
36  
37  
38  
39  
40 To date, several classes of FABP4 inhibitors have been identified for therapeutic  
41 intervention in diseases like insulin resistance, type 2 diabetes and atherosclerosis.<sup>20-32</sup>  
42 BMS309403, the prime inhibitor of FABP4 developed by Bristol-Myers Squibb, has  
43 been used to explore its anti-inflammatory effect *in vitro* and *in vivo*. It was shown that  
44 BMS309403 decreased the production of pro-inflammatory cytokines and alleviated  
45 the LPS-induced acute lung injury, non-alcoholic steatohepatitis, and renal interstitial  
46 fibrosis.<sup>12-15,33,34</sup> However, compared to the knockout of FABP4, the anti-inflammatory  
47 efficacy of BMS309403 was unsatisfied.<sup>7,8</sup> It is noteworthy that binding affinities of  
48 most available inhibitors are equivalent to that of FAs such as palmitic acid and linoleic  
49 acid.<sup>16</sup> As a result, it is difficult for these inhibitors to compete with FAs which are

1  
2  
3  
4 often at a high level *in vivo*. Therefore, it is worth identifying more potent FABP4  
5 inhibitors to systematically explore the effectiveness of FABP4 in anti-inflammation  
6 and to provide novel compounds possessing more-drug-like properties.  
7  
8  
9

10 Herein, with a fragment-based lead discovery strategy, we sought to design and  
11 synthesize a new class of potent FABP4 inhibitors, and therapeutic potentials of the  
12 inhibitors in treating systemic inflammatory response syndrome were explored. To find  
13 a hit with a new scaffold, we screened our in-house 500-fragment library and identified  
14 an interesting hit (fragment **1**) with multiple binding poses shown in the ligand binding  
15 pocket of FABP4. With the aid of the determined crystal structures and binding  
16 affinities, a series of 2-(phenylamino)benzoic acids as novel and potent FABP4  
17 inhibitors were successfully designed on basis of this weak fragment binder. In the  
18 following, we comprehensively illustrate the hit discovery, a hit-to-lead optimization  
19 and evaluation of potency, selectivity, pharmacokinetic properties, and anti-  
20 inflammatory efficacy of the inhibitors.  
21  
22  
23  
24  
25  
26  
27  
28  
29  
30  
31  
32

## 33 ■ RESULTS AND DISCUSSION

34  
35  
36 **Hit Identification and Characterization.** Given the advantage of fragment-  
37 screening campaigns in hit/lead discovery,<sup>35,36</sup> an in-house 500-fragment collection was  
38 screened against human FABP4 using the 8-anilino-1-naphthalene-sulfonic acid (1,8-  
39 ANS) displacement assay. The concentration of fragments used for the testing is 1 mM.  
40 Two analogs of benzoic acid, fragments **1** (MW = 214.2,  $K_i = 50.7 \mu\text{M}$ ) and **2** (MW =  
41 213.2,  $K_i > 500 \mu\text{M}$ ), were identified as FABP4 binders. Encouraged by a high ligand-  
42 binding efficiency of fragment **1** (LE = 0.36), we carried out a structure-based hit-to-  
43 lead optimization on this diphenylamine scaffold in order to discover novel, highly  
44 potent and selective FABP4 inhibitors. However, the endogenous FAs bound in the  
45 ligand binding pocket of FABP4 and the relatively weak binding affinity of **1** impeded  
46 the complex structure determination. In this scenario, we tried to remove the  
47 endogenous FAs from FABP4 through a denaturation and refolding of the recombinant  
48  
49  
50  
51  
52  
53  
54  
55  
56  
57  
58  
59  
60

1  
2  
3  
4 FABP4. To solve the structure of FABP4 in complex with fragment **1**, crystals of apo  
5  
6 FABP4 obtained at pH 6.5 and 7.5 were soaked with the fragment. To our surprise, the  
7  
8 complex structures show that fragment **1** adopts more than one binding pose in the  
9  
10 ligand binding pocket of FABP4. According to the electron density map, three different  
11  
12 but partially overlapped binding poses of **1** could be fitted (Figures 1A and S1). At pH  
13  
14 6.5, two poses (Pose 1 and Pose 2) are found in the pocket (Figure S1A). Pose 1 presents  
15  
16 a classical binding mode which is utilized by most FABP4 inhibitors. With such a pose,  
17  
18 the carboxylic group forms multiple polar interactions with R126 as well as Y128, and  
19  
20 the free phenyl ring mainly establishes face-to-edge  $\pi$ -stacking interactions with F16  
21  
22 (Figure 1B). However, in Pose 2, the carboxylic group forms hydrogen bonds (H-bonds)  
23  
24 to S53 and T60 directly, and to S55, K58 and A75 through water molecules (Figure  
25  
26 1C). Besides, the phenyl ring of the benzoic acid group interacts with F57 via a  $\pi$ - $\pi$   
27  
28 stacking, while the free phenyl ring occupies a position as that seen in Pose 1 to form  
29  
30 face-to-edge  $\pi$ -stacking interactions with F16. The difference electron-density map  
31  
32 suggests that Pose 2 (occupancy = 0.58) is more stable than Pose 1 (occupancy = 0.42)  
33  
34 in the crystal structure determined at pH 6.5 (Figure S1A). There are also two binding  
35  
36 poses of the fragment found in the complex structure determined at pH 7.5. One is Pose  
37  
38 2 although its occupancy (0.41) is relatively low. The second one is a new pose, Pose 3  
39  
40 (occupancy = 0.59) (Figure S1B). Similar to Pose 1, the carboxylic group of the benzoic  
41  
42 acid in Pose 3 forms polar interactions with R126 and Y128, while the free phenyl ring  
43  
44 flips up to form hydrophobic interactions with F57 and A75 (Figure 1D). Taken  
45  
46 together, two crystal structures of FABP4 in complex with fragment **1** reveal three  
47  
48 possible binding poses of the fragment, suggesting that this fragment in the ligand  
49  
50 binding pocket is mobile and may switch from one pose to another.  
51  
52  
53  
54  
55  
56  
57  
58  
59  
60

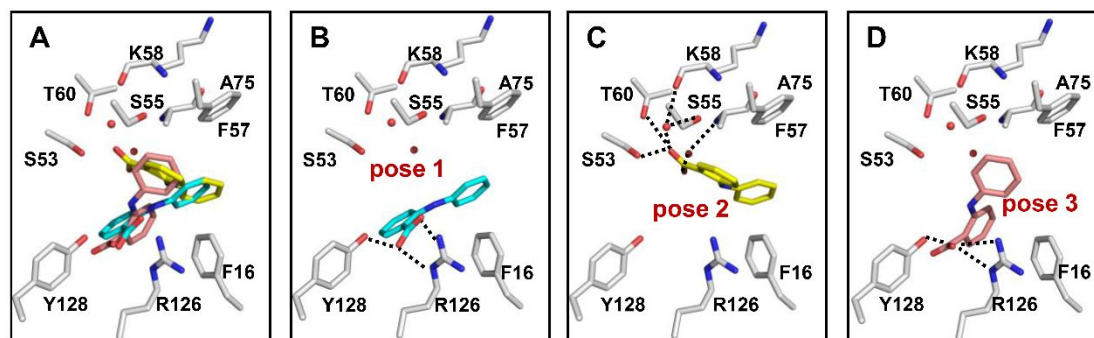


**Figure 1.** Crystal structures of FABP4 in complex with fragment **1** determined at pH 6.5 and 7.5 (PDB codes: 6LJW and 6LJX). (A) An overlay of three binding poses of **1** shown in B-D. (B-D) A representation of Pose 1 (B), Pose 2 (C) and Pose3 (D). Residues interacting with **1** are shown as gray sticks and H-bonds are represented by black dashed lines.

Although the occupancy of Pose 1 in the crystal structure is low, it is similar to the typical binding mode utilized by other FABP4 inhibitors, in which F16, R126 and Y128 are the key residues for the ligand binding.<sup>16</sup> To further explore the probability of Pose 1 and investigate the dynamic behavior of fragment **1** inside FABP4, molecular dynamic (MD) simulations were performed on Pose 1 in complex with FABP4.<sup>16</sup> As expected, the fragment is mobile during the simulation and its root mean square deviations (RMSDs) fluctuate from 1.0 to 7.0 Å, while the backbone RMSDs of FABP4 have a relatively smooth fluctuation around 2.0 Å (Figure 2). After a cluster analysis on conformations of the fragment extracted from the MD trajectory, four major conformations (I to IV) are found and their representative snapshots superimposed to three poses in the crystal structures are displayed in Figure 2. It seems that conformations I and III are very close to Poses 1 and 3, with averaged RMSDs of 2.0 and 1.3 Å, respectively. Conformation II is similar to Pose 2 but with a relatively larger RMSD (2.9 Å). Conformation IV of the fragment is distinctive to three poses (RMSDs > 4.6 Å), although the benzoic acid moiety is similar to that of Pose 3. Accordingly, starting with Pose 1, the fragment can move to conformations almost identical to Pose 2 and Pose 3 during the 600-ns MD simulation, demonstrating again that the binding of fragment **1** with FABP4 is mobile and the multiple bound conformations could be

exchanged one another.

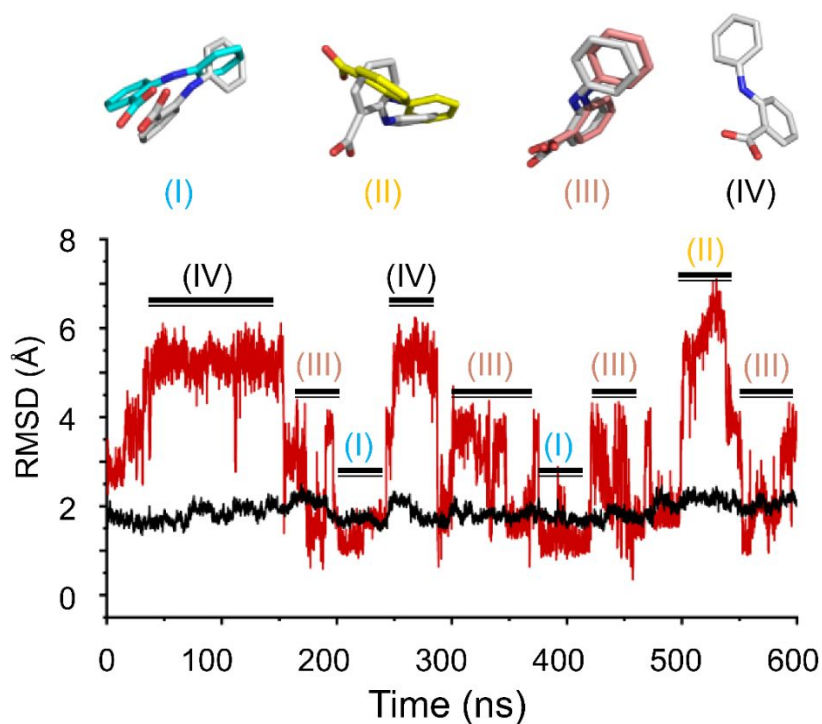


**Figure 2.** An overlay of representative conformations of fragment **1** extracted from the MD trajectory (gray sticks) with three poses shown in the crystal structures (Pose 1: cyan sticks; Pose 2: yellow sticks; Pose 3: pink sticks). RMSDs of backbone atoms of FABP4 (black) and all atoms of fragment **1** (red) versus the simulation time were calculated based on the MD trajectory.

**Micromolar-to-Nanomolar Potency Improvement.** Though fragment **1** employs multiple conformations to interact with FABP4, the essential amino acids participating in binding include F16, S53, F57, R126, and Y128. This gave us a valuable clue to rationally design more potent inhibitors with full consideration of interactions with these residues. In addition, two phenyl rings of the fragment are overlapped each other in three binding poses, resulting in three location of the phenyl rings (Figure 1A and 3A). In order to obtain a new compound containing three phenyl rings so as to simultaneously occupy the overlapped position of phenyl rings in three poses, we added a benzene ring to C13 of Pose **1** (Figure 3A). The resulting 2-([1,1'-biphenyl]-2-

1  
2  
3  
4  
5  
6  
7  
8  
9  
10  
11  
12  
13  
14  
15  
16  
17  
18  
19  
20  
21  
22  
23  
24  
25  
26  
27  
28  
29  
30  
31  
32  
33  
34  
35  
36  
37  
38  
39  
40  
41  
42  
43  
44  
45  
46  
47  
48  
49  
50  
51  
52  
53  
54  
55  
56  
57  
58  
59  
60

ylamino)benzoic acid (**3**) has a  $K_i$  of 109.3 nM, which is a ~460-fold increase in  $K_i$  compared to fragment **1** (Table 1). It is also more potent than the well-studied BMS309403 with a  $K_i$  of 253.4 nM. Attachment of an anilino (**4**) or a phenoxy group (**5**) to C13 of **1** also shows a modest increase in the binding affinity, but they are much less potent than compound **3**. The complex structure of FABP4 bound with **3** reveals that three phenyl rings take positions as they are in three binding poses of fragment **1**, and the binding pose of compound **3** is more like a hybrid of Pose 1 and Pose 2 (Figures 1 and 3B). The added phenyl ring extends to a position which was once occupied by the benzoic acid moiety of Pose 2 or the free phenyl ring of Pose 3. This ring of **3** simultaneously participates in an edge-to-face  $\pi$ - $\pi$  stacking interactions with F57 and cation- $\pi$  interactions with R126. The rest part of **3** adopts a conformation similar to that in Pose 1. The carboxylic group makes H-bonds with R126 and Y128 directly, and with S53 through a water molecule, while the middle phenyl ring forms face-to-edge  $\pi$ -stacking interactions with F16 (Figures 3B,C). These interactions between three phenyl rings as well as the carboxylic group of **3** and five key residues (F16, S53, F57, R126, and Y128) account for the huge improvement of potency for compound **3** relative to fragment **1**, demonstrating the rational for design of compound **3**. However, inserting an additional NH and O between two phenyl rings in compounds **4** and **5**, respectively, might generate clashes with the neighboring residues and result in remarkably reduced potency (Table 1). In summary, the hybrid of the binding poses of fragment **1** leads to efficiently design a novel and potent inhibitor of FABP4 by only adding a phenyl ring to the right position of fragment **1**.

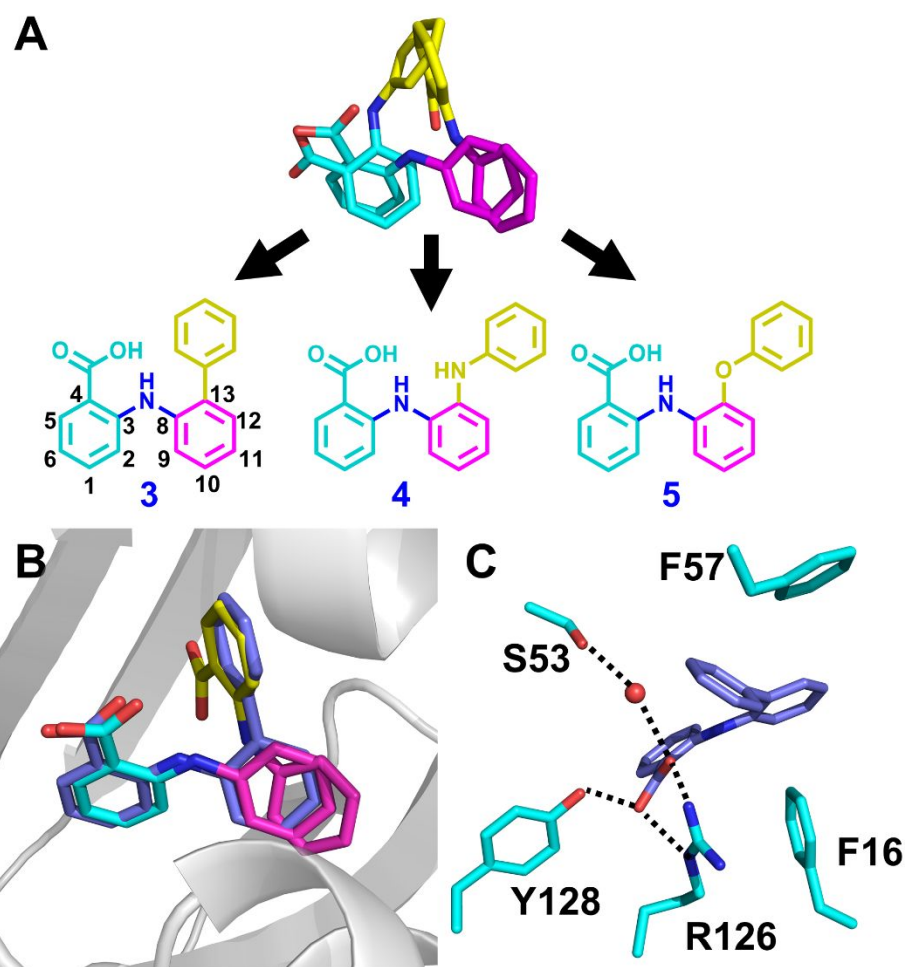
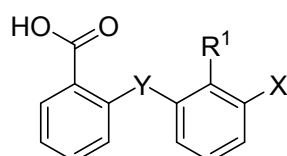


**Figure 3.** (A) Design of new inhibitors based on an overlay of different binding poses of fragment **1**. (B) An overlay of the binding poses of compound **3** (purple sticks) and fragment **1** by superimposing crystal structures of FABP4 in complex with **3** and **1**. (C) Interactions of **3** with the surrounding residues revealed by the crystal structure (PDB code: 6LJS). Residues are shown as cyan sticks and H-bonds are represented by black dashed lines.

**Binding Affinities Determined by ITC.** Given that the concentration of FABP4 used in the 1,8-ANS displacement assay is  $\sim 0.8 \mu\text{M}$ , the detection limit of  $\text{IC}_{50}$  with this assay is over  $0.4 \mu\text{M}$ . Therefore, this assay usually measures  $K_i$  values over  $77.4 \text{ nM}$  according to the equation  $K_i = \text{IC}_{50}/(1+[1,8\text{-ANS}]/K_d)$ , where  $[1,8\text{-ANS}]$  is the concentration of 1,8-ANS used in the assay and  $K_d$  means the dissociating constant for 1,8-ANS with FABP4. We found that the  $K_i$  of compound **3** ( $109.3 \text{ nM}$ ) is close to the

detection limit of the 1,8-ANS displacement assay. This makes it difficult to use this assay to precisely determine the binding affinity of more potent inhibitors derived from compound **3**. Isothermal titration calorimetry (ITC), widely known as an invaluable tool to determine thermodynamic parameters of protein-ligand interactions, is also frequently used to obtain  $K_d$  values ranging from  $10^{-3}$  M to  $10^{-8}$  M. To gain the accurate binding affinity of the inhibitors with FABP4, ITC measurements were employed to determine the  $K_d$  values of the compounds, in particular for the binding affinities of those compounds ( $IC_{50} < 0.5 \mu\text{M}$ ,  $K_i < 96.8 \text{ nM}$ ) close to or even beyond the detection limit of the 1,8-ANS displacement assay. The ITC measured  $K_d$  of compound **3** binding to apo FABP4 is 110.6 nM, which is also stronger than that of BMS309403 (252.7 nM).

**Table 1. Effects of X, Y and R<sup>1</sup> substitutions on binding affinities of compounds with FABP4<sup>a</sup>**



Compound	X	Y	R <sup>1</sup>	$K_i$ or $K_d$ (nM)	MW	LE
<b>1</b>	H	NH	H	$50690.3 \pm 4326.7^b$	213.2	0.36
<b>2</b>	H	O	H	$> 500000^b$	214.2	$< 0.27$
<b>3</b>	H	NH		$109.3 \pm 0.6^b$	289.3	0.43
				$110.6 \pm 8.8^c$		0.43
<b>4</b>	H	NH		$3741.9 \pm 201.3^b$	304.3	0.32
<b>5</b>	H	NH		$1476.0 \pm 189.5^b$	305.3	0.34
<b>6</b>	Cl	NH		$34.4 \pm 7.5^c$	323.8	0.43
<b>7</b>	Br	NH		$262.9 \pm 11.0^b$	368.2	0.39

8	CF <sub>3</sub>	NH		164.1 ± 4.5 <sup>b</sup>	357.3	0.35
9	CH <sub>3</sub>	NH		182.4 ± 4.4 <sup>b</sup>	303.4	0.40
10	OCH <sub>3</sub>	NH		43.9 ± 5.1 <sup>c</sup>	319.4	0.41
<b>BMS309403</b>				253.4 ± 21.2 <sup>b</sup>	474.5	0.25
				252.7 ± 30.7 <sup>c</sup>		0.25

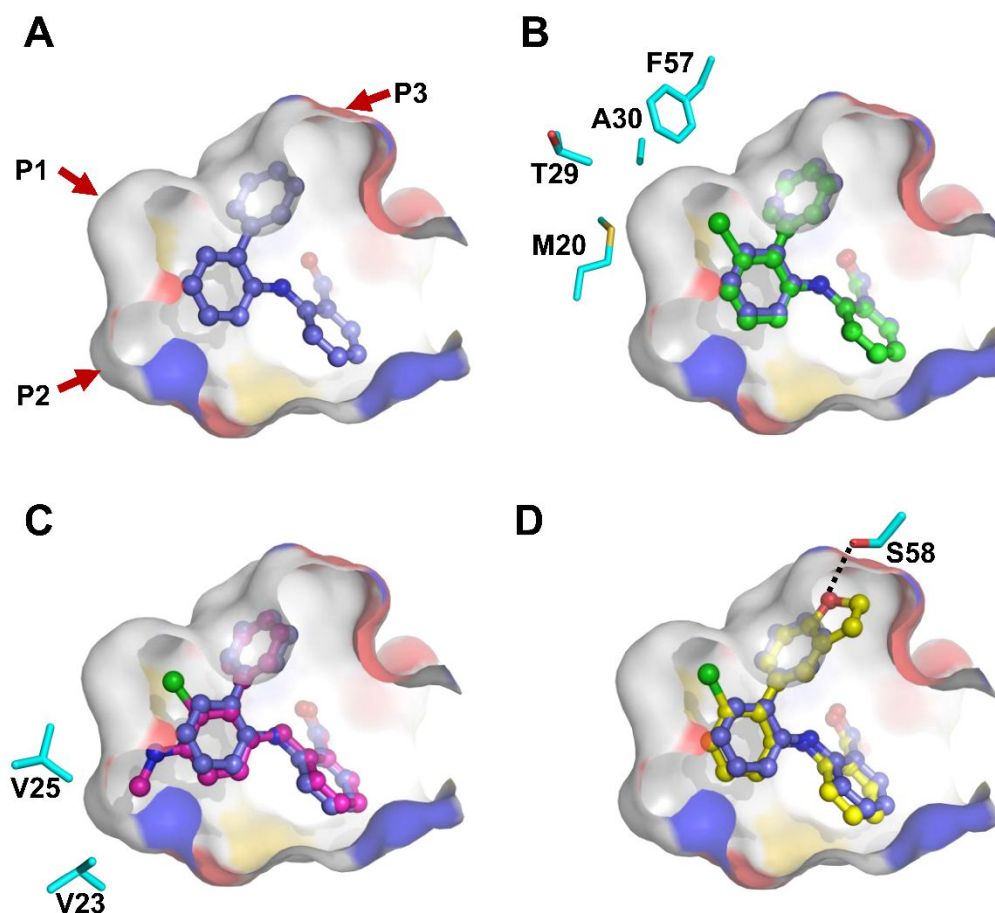
<sup>a</sup> The values of  $K_i$  or  $K_d$  were expressed as mean ± SD based on three independent experiments and determined via the nonlinear regression analysis using GraphPad Prism software 8.0.

<sup>b</sup>  $K_i$  measured by the 1,8-ANS displacement assay

<sup>c</sup>  $K_d$  measured by ITC

**Optimization Based on Compound 3.** Inspired by the above results, we embarked on an optimization around the [1,1'-biphenyl]-2-amine scaffold rather than the benzoic acid moiety of compound **3**. The crystal structure of FABP4-**3** reveals that small cavities appear near atoms C11 and C12. It looks like that substituents with a small size are suitable to fill these cavities. To test this, introducing various substituents at C12 (the X substituent) was conducted in order to find the right substituent matching the hydrophobic cavity defined by M20, T29 and F57 (Site P1) (Figure 4A and Table 1). Compared to the unsubstituted **3**, introduction of a chloro (compound **6**) or a methoxy (compound **10**) group results in higher binding affinities. In particular, the chloro-substituted compound (**6**,  $K_d = 34.4$  nM) yields an approximately 3-fold increase in affinity compared to compound **3** (Table 1). However, introduction of a bromo (compound **7**), a trifluoromethyl (compound **8**) or a methyl (compound **9**) at the same position decreases the binding affinities compared to compound **3**. The determined crystal structure of FABP4 in complex with **6** shows the protein-ligand interactions seen in the FABP4-**6** complex are almost identical to those in the FABP4-**3** complex, except that the chloro group in **6** forms favorable hydrophobic interactions with the surround residues such as M20, T29, A30, and F57 (Figure 4B). Besides the size of the substituent groups, the compounds attached with the electron-withdrawing substituents

1  
2  
3  
4 tend to be more potent compared to their counterparts, for example, **8** versus **9**.  
5  
6 Accordingly, the chloro group, with an appropriately size and a negative inductive  
7  
8 effect, was identified as the favorable substituent of X for a further optimization.  
9  
10  
11  
12



43  
44  
45  
46  
47  
48  
49  
50  
51  
52  
53  
54  
55  
56  
57  
58  
59  
60

**Figure 4.** X-ray crystal structures of FABP4 in complex with compounds **3** (purple, A; PDB code: 6LJS), **6** (green, B; PDB code: 6LJT), **11** (magenta, C; PDB code: 6LJU), and **17** (yellow, D; PDB code: 6LJV). Sites P1, P2 and P3 show the optimization directions. The ligand binding pocket is presented by molecular surface. The dashed lines indicate H-bonds between compounds and residues.

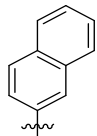
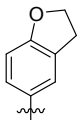
**Optimization Based on Compound 6.** The crystal structure of FABP4-**6** also reveals that a region defined by V23 and V25 (Site P2) could potentially accommodate the substituents at C11 of **6** (Figure 4A,B). Considering the synthesis feasibility and the selectivity for FABP4 over FABP3, several aliphatic amine substituted compounds

1  
2  
3  
4 were designed, synthesized and evaluated (Table 2). The most potent compound is **11**  
5 ( $K_d = 60.1$  nM), which is slightly less potent than **6**. The determined crystal structure of  
6 FABP4 in complex with compound **11** suggests that this compound adopts a binding  
7 pose almost identical to **6** and the introduced methyl group establishes hydrophobic  
8 interactions with V23 and V25 (Figure 4C). The underlying mechanism accounting for  
9 the lower potency of **11** over **6** may be ascribed to the electron-donating ability of the  
10 aliphatic amine substituents, which are helpful to dense the  $\pi$ -electron density and  
11 thereby are harmful to the  $\pi$ - $\pi$  interactions between the attached benzene ring and F16.  
12 However, compounds **12** and **13**, decorated with a bulkier *N,N*-dimethylamino and  
13 ethylamino group, respectively, show a remarkably reduced potency compared to **11**.  
14 It is thus suggested that the *N,N*-dimethylamino or ethylamino group is too large to  
15 compatible with Site P2.  
16  
17  
18  
19  
20  
21  
22  
23  
24  
25  
26  
27

28 Another small region could be exploited by our inhibitors is Site P3 which is around  
29 the free phenyl ring of **6** (Figure 4A). Aiming to engage more favorable interactions  
30 with the neighboring residues and maintain the binding pose of **6**, the free phenyl ring  
31 of **6** was replaced by various bicyclic rings. Six synthesized compounds (**14**~**19**) retain  
32 high binding affinities with FABP4. Among them, the most potent one, compound **17**,  
33 has a  $K_d$  of 37.4 nM which nearly equals to the  $K_d$  of **6** (Table 2). The binding mode of  
34 **17** with FABP4 was also determined by the X-ray protein crystallography (Figure 4D).  
35 As expected, the bound pose of **17** is overlapped well with that of **6** and an additional  
36 H-bond is observed between the hydroxyl group of S55 and the oxygen atom of the  
37 dihydrofuran ring in **17**. Increase of aromaticity of the bicyclic rings reduces the binding  
38 affinities of compounds **14**, **15**, **18**, and **19** with FABP4. Introducing the second oxygen  
39 into the bicyclic ring also results in a lower binding affinity of **16** compared to **17** (136.2  
40 nM versus 37.4 nM). Overall, small modification of the free phenyl ring of **6** so as to  
41 fill the neighbouring space leads to discovery of a novel and potent inhibitor (**17**) with  
42 a binding affinity comparable to that of **6**.  
43  
44  
45  
46  
47  
48  
49  
50  
51  
52  
53  
54  
55  
56  
57  
58  
59  
60

**Table 2. Effects of R<sup>1</sup> and R<sup>2</sup> substituents on binding affinities of compounds with FABP4<sup>a</sup>**

Compound	R <sup>1</sup>	R <sup>2</sup>	<i>K<sub>i</sub></i> or <i>K<sub>d</sub></i> (nM)	MW	LE
<b>6</b>		H	34.4 ± 7.5 <sup>c</sup>	323.8	0.43
<b>11</b>			60.1 ± 9.2 <sup>c</sup>	352.8	0.39
<b>12</b>			826.4 ± 22.8 <sup>b</sup>	366.8	0.32
<b>13</b>			1525.0 ± 54.4 <sup>b</sup>	366.8	0.30
<b>14</b>		H	96.2 ± 4.5 <sup>c</sup>	363.8	0.36
<b>15</b>		H	125.5 ± 22.5 <sup>c</sup>	365.8	0.36
<b>16</b>		H	136.2 ± 2.7 <sup>c</sup>	367.8	0.36
<b>17</b>		H	37.4 ± 7.4 <sup>c</sup>	365.8	0.39
<b>18</b>		H	90.1 ± 18.3 <sup>c</sup>	363.8	0.37

19		H	$149.7 \pm 28.7^b$	373.8	0.34
20			$58.4 \pm 3.6^c$	394.9	0.35

<sup>a</sup> The values of  $K_i$  or  $K_d$  were expressed as mean  $\pm$  SD from three independent experiments and determined via the nonlinear regression analysis using GraphPad Prism software 8.0.

<sup>b</sup>  $K_i$  measured by 1,8-ANS displacement assay.

<sup>c</sup>  $K_d$  measured by ITC

**Selectivity.** Considering the side effect caused by the inhibitory activity of compounds against the cardiac form of FABP (FABP3), compounds that show a great binding affinity with FABP4 were examined for their affinities with FABP3 by the 1,8-ANS displacement assay. BMS309403 was used as a positive control. The data listed in Table 3 shows that several compounds (**3**, **6**, **10**, **11**, **17**, and **20**) have a good selectivity for FABP4 over FABP3 and their selectivity indexes are superior or similar to BMS309403. In particular, compound **11** exhibits a 238-fold selectivity for FABP4 over FABP3, which is significantly more selective than BMS309403 (29-fold). In order to understand the structural basis for the different selectivity index of the compounds, crystal structures of FABP4 and FABP3 were superimposed (Figure S2). Residue V23 is in close proximity to and forms hydrophobic interactions with the methylamino group of **11** in the FABP4-**11** complex while it is a leucine at the same position in FABP3. A larger side-chain of L23 in FABP3 might create a steric hindrance for the binding of the methylamino group, resulting in a weak binding of **11** with FABP3. In contrast, without the methylamino group, compound **6** has a lower selective index, though it has a stronger binding affinity with FABP4. Stimulated by the high selectivity index of **11**, the methylamino group was added to the C11 of compound **17**, whose binding affinity is similar to that of **6**, to yield compound **20**. As expected, **20** does exhibit a much higher selectivity index for FABP4 over FABP3 compared to **17**, while its binding affinity to FABP4 is slightly less than that of **17**. Therefore, the methylamino substitution on C11

in the middle phenyl ring plays a key role in improving the selectivity of this series of compounds toward FABP4 over FABP3. It should be noted that other factors can also affect the selectivity index. For example, compound **3** without such a methylamino substitution also has a selectivity index of 117. Taken together, compounds **3**, **6**, **10**, **11**, **17**, and **20** show high affinity with FABP4 and favorable selectivity for FABP4 over FABP3.

In addition, the binding affinities of these inhibitors with FABP5 were examined. It shows that compounds **6**, **14**, **15**, **17**, **18**, and **19** have a good binding affinity with FABP5.

**Table 3. Selectivity of the FABP4 Inhibitors toward FABP3 and FABP5.**

Compound	FABP3 $K_i$ ( $\mu\text{M}$ ) <sup>a</sup>	FABP5 $K_i$ ( $\mu\text{M}$ ) <sup>a</sup>	FABP3/FABP4 <sup>b</sup>
<b>BMS309403</b>	7.45 ± 0.28	9.24 ± 0.21	29
<b>3</b>	12.82 ± 1.91	8.23 ± 0.42	117
<b>6</b>	1.00 ± 0.17	0.88 ± 0.06	29
<b>10</b>	1.51 ± 0.02	1.20 ± 0.12	34
<b>11</b>	14.29 ± 0.24	17.75 ± 0.92	238
<b>14</b>	0.74 ± 0.02	0.49 ± 0.01	8
<b>15</b>	1.50 ± 0.04	0.60 ± 0.04	12
<b>16</b>	0.86 ± 0.08	1.07 ± 0.04	6
<b>17</b>	1.40 ± 0.13	0.82 ± 0.02	37
<b>18</b>	0.35 ± 0.01	0.43 ± 0.01	4
<b>19</b>	1.42 ± 0.03	0.60 ± 0.04	9
<b>20</b>	9.62 ± 0.63	32.04 ± 1.63	165

<sup>a</sup> The values of  $K_i$  were expressed as mean ± SD based on three independent experiments and determined via the nonlinear regression analysis using GraphPad Prism software 8.0.

<sup>b</sup> Selectivity index was resulted from the  $K_i$  of a compound with FABP3 divided by  $K_i$  or  $K_d$  of the compound with FABP4.

**Anti-inflammatory Effects on THP-1 Macrophages.** Genetic ablation or pharmacological inhibition of FABP4 has been demonstrated to attenuate inflammatory

responses in macrophages.<sup>8,10</sup> Therefore, we selected several compounds with high affinity with FABP4 and favorable selectivity for FABP4 over FABP3 to explore their anti-inflammatory effect on the LPS-stimulated THP-1 macrophages. Firstly, the cytotoxicity was evaluated with a CCK-8 assay, and the result shows that all tested compounds (**3**, **6**, **10**, **11**, **17**, and **20**) at 20  $\mu\text{M}$  and 50  $\mu\text{M}$  have no effect on the cell viability of THP-1 macrophages (Figure S3A). Next, THP-1 macrophages were incubated with these compounds at 20  $\mu\text{M}$  for 18 h followed by a LPS stimulation for another 6 h. As shown in Figure S3B and S3C, the application of LPS resulted in a dramatic increase in secretion of pro-inflammatory cytokines, MCP-1 and IL-6, and our compounds as well as BMS309403 attenuated the inflammatory responses by reducing the level of MCP-1 and IL-6. Among these compounds, **17** exhibits the best *in vitro* anti-inflammatory efficacy in the LPS-stimulated THP-1 macrophages and it is thus chosen for a further study. As illustrated in Figure 5, compound **17** inhibited both MCP-1 and IL-6 release from the LPS-stimulated THP-1 macrophages in a dose-dependent manner, and its efficacy is even superior to BMS309403. Taken together, these results suggest that our compounds possess an anti-inflammatory effect on the LPS-stimulated THP-1 macrophages and the efficacy of compound **17** is even better than that of BMS309403.

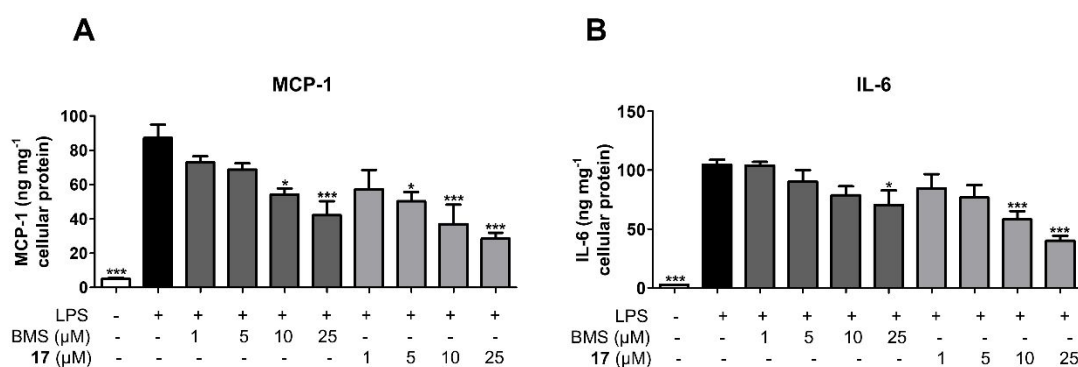


**Figure 5.** Effects of BMS309403 and compound **17** on the secretion of pro-inflammatory cytokines, MCP-1 (A) and IL-6 (B), in the LPS-stimulated THP-1 macrophages. MCP-1 and IL-6 were measured by the Elisa Kits. Data are given as mean  $\pm$  standard error of the mean (SEM) of three independent experiments. Statistical analysis is performed by one-way analysis of variance

(ANOVA). \* $P < 0.05$ , \*\*\* $P < 0.001$  vs LPS group.

**Lipolysis Inhibition in 3T3-L1 Adipocytes.** As previously reported, ablation or chemical inhibition of FABP4 decreases lipolysis in adipocytes,<sup>27,37</sup> hence, we also investigated the effects of compound **17** on adipocyte lipolysis. Again, the CCK-8 assay was first carried out to test the cytotoxicity of the compounds. It shows that both BMS309403 and **17** have no significant cytotoxicity on 3T3-L1 adipocytes at any tested concentration (Figure S4). The lipolysis experiment was then conducted at various concentrations of tested compounds and the result is shown in Figure 6. The lipolytic inhibition by compound **17** was more significant than that of the positive control, BMS309403. These results further confirm the efficacy of compound **17** on the lipolysis inhibition in 3T3-L1 adipocytes by binding to FABP4.

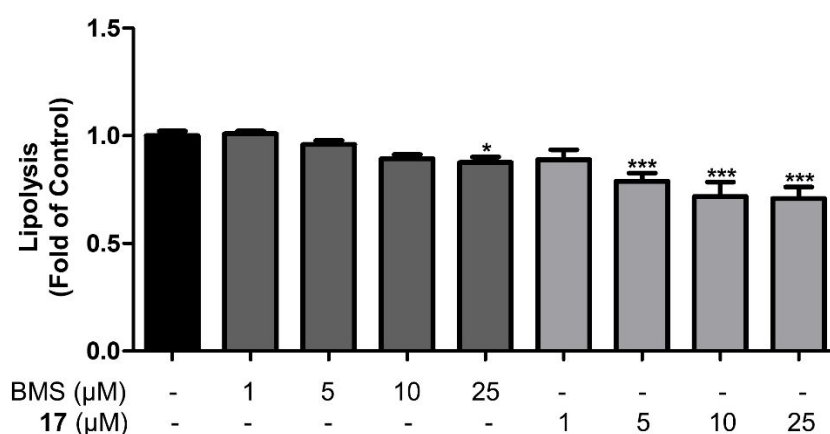


**Figure 6.** Effect of BMS309403 and compound **17** on the release of free glycerol from the forskolin-stimulated mature 3T3-L1 adipocytes. Data are given as mean  $\pm$  SEM of at least three independent experiments, and each is performed in triplicate. Statistical analysis is performed by one-way ANOVA. \* $P < 0.05$ , \*\*\* $P < 0.001$  vs Control group.

***In Vitro* ADME and *in Vivo* PK Properties of **17**.** Compound **17**, with an excellent inhibitory activity against FABP4 both at molecular and cellular level, was progressed to an *in vivo* efficacy study. Before that, the metabolic stability of **17** were evaluated using mouse and human liver microsomes. Table 4 shows that **17** is relatively stable in

the human and mouse liver microsomes. Furthermore, the Caco-2 cell permeability experiment implies that **17** possesses a good cell permeability *in vitro* with a low efflux ratio of 0.21.

The PK properties of compound **17** were preliminary evaluated in mice with an intravenous (3 mg/kg) and oral (10 and 25 mg/kg) administration. The results are shown in Table 5. After an oral delivery of **17** at a dose of 25 mg/kg, it exhibits an acceptable PK profile with a  $T_{1/2}$  of 3.82 h, a favorable area under curve (AUC) of 43.77  $\mu\text{g}\cdot\text{h/mL}$ , a good oral bioavailability of 57.0%, and a good plasma duration (MRT) of 3.1 h. Together, these data imply that compound **17** is suitable for *in vivo* efficacy evaluation.

**Table 4. Metabolic Stability in Liver Microsomes and Caco-2 Permeability of 17**

	Parameter	Value
	$T_{1/2}$ (min, Human)	86.5
Metabolic Stability in Liver Microsomes	$T_{1/2}$ (min, Mouse)	112.2
	$CL_{\text{int}}$ (mL/min/gprot, Human)	24.3
	$CL_{\text{int}}$ (mL/min/gprot, Mouse)	18.7
Caco-2 permeability	$P_{\text{app}}(\text{A-B})$ ( $10^{-6}$ cm/s)	6.23
	Efflux ratio	0.21

**Table 5. PK Profile of 17 in Mice**

Administration	p.o.		i.v.
	(10 mg/kg)	(25 mg/kg)	(3 mg/kg)
$T_{1/2}$ (h)	4.77 $\pm$ 0.76	3.82 $\pm$ 0.29	5.76 $\pm$ 0.40
$T_{\text{max}}$ (h)	0.25 $\pm$ 0.00	0.25 $\pm$ 0.00	
$C_{\text{max}}$ ( $\mu\text{g/mL}$ )	3.43 $\pm$ 1.66	12.99 $\pm$ 1.78	
$\text{AUC}_{0-24\text{h}}$ ( $\mu\text{g}\cdot\text{h/mL}$ )	12.8 $\pm$ 3.51	43.77 $\pm$ 5.53	9.38 $\pm$ 3.57
CL (mL/min/kg)			5.80 $\pm$ 1.86

V <sub>ss</sub> (L/kg)			1.65 ± 0.46
MRT (h)	7.59 ± 1.33	6.55 ± 0.12	4.83 ± 0.69
F (%)	40.9	57.0	

***In Vivo* Anti-Inflammatory Efficacy Study.** As compound **17** exhibits excellent anti-inflammatory effects in the LPS-stimulated THP-1 macrophages and a satisfying performance in liver microsomes stability and PK properties, we next explored its anti-inflammatory effect *in vivo*. C57BL/6J mice were intragastrically administrated with BMS309403 or compound **17** at a dose of 50 mg/kg 1 h before a single intraperitoneal injection of LPS at a dose of 5 mg/kg. Concentrations of MCP-1 and IL-6 in serum were measured 5 h after LPS injection. As shown in Figure 7, LPS treatment dramatically increases the level of inflammatory cytokines such as MCP-1 and IL-6 in the serum of vehicle mice, while an oral administration of BMS309403 or compound **17** prominently downregulate the secretion of MCP-1 and IL-6. Consistent with the *in vitro* results noted above, the anti-inflammatory efficacy of compound **17** *in vivo* is also more significant than that of BMS309403, demonstrating the anti-inflammatory potential of compound **17**.

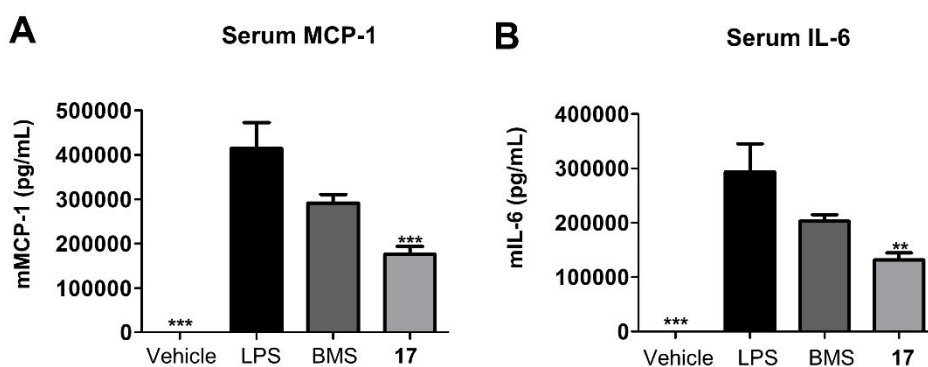


**Figure 7.** Effects of BMS309403 (50 mg/kg) and compound **17** (50 mg/kg) on the secretion of pro-inflammatory cytokines, MCP-1 (A) and IL-6 (B), in the serum of LPS-treated C57BL/6J mice (n = 8 mice/group). MCP-1 and IL-6 were measured by the Elisa Kits. Data are given as mean ± SEM and statistical analysis is performed by one-way ANOVA. \*\*  $P < 0.01$ , \*\*\*  $P < 0.001$  vs LPS group.

**Efficacy of Compound 17 for Multi-Organ Protection.** To explore the effect of

1  
2  
3  
4 compound **17** on organ damage, C57BL/6J mice were intragastrically administrated  
5 with BMS309403 (25 mg/kg) or **17** (10, 25 and 50 mg/kg) once a day for consecutive  
6 four days prior to a single LPS intraperitoneal injection at a dose of 10 mg/kg. As shown  
7 in Figure 8A, the level of liver damage markers, serum aspartate aminotransferase (AST)  
8 as well as alanine transaminase (ALT), and of a kidney damage marker, blood urea  
9 nitrogen (BUN), are significantly increased after the injection of LPS compared with  
10 the vehicle mice. In contrast, administration of compound **17** decreases the level of  
11 these biomarkers in a dose-dependent manner, which is equivalent to or even better  
12 than BMS309403, indicating a beneficial effect of compound **17** on hepatorenal  
13 function. In addition, the histological staining results can clearly interpret organ damage  
14 which is manifested as the infiltration of inflammatory cells and damaged cells.  
15 Compared with the LPS-treated mice, BMS309403 and compound **17**-treated mice  
16 have a limited extent of damage in key organs such as lung, liver, kidney, and spleen,  
17 which are close to those of healthy animals (Figure 8B). Taken together, these results  
18 indicate that compound **17** is able to effectively attenuate a systemic inflammatory  
19 damage and acts as a good candidate for the treatment of inflammation-related diseases.  
20  
21  
22  
23  
24  
25  
26  
27  
28  
29  
30  
31  
32  
33  
34  
35  
36  
37  
38  
39  
40  
41  
42  
43  
44  
45  
46  
47  
48  
49  
50  
51  
52  
53  
54  
55  
56  
57  
58  
59  
60

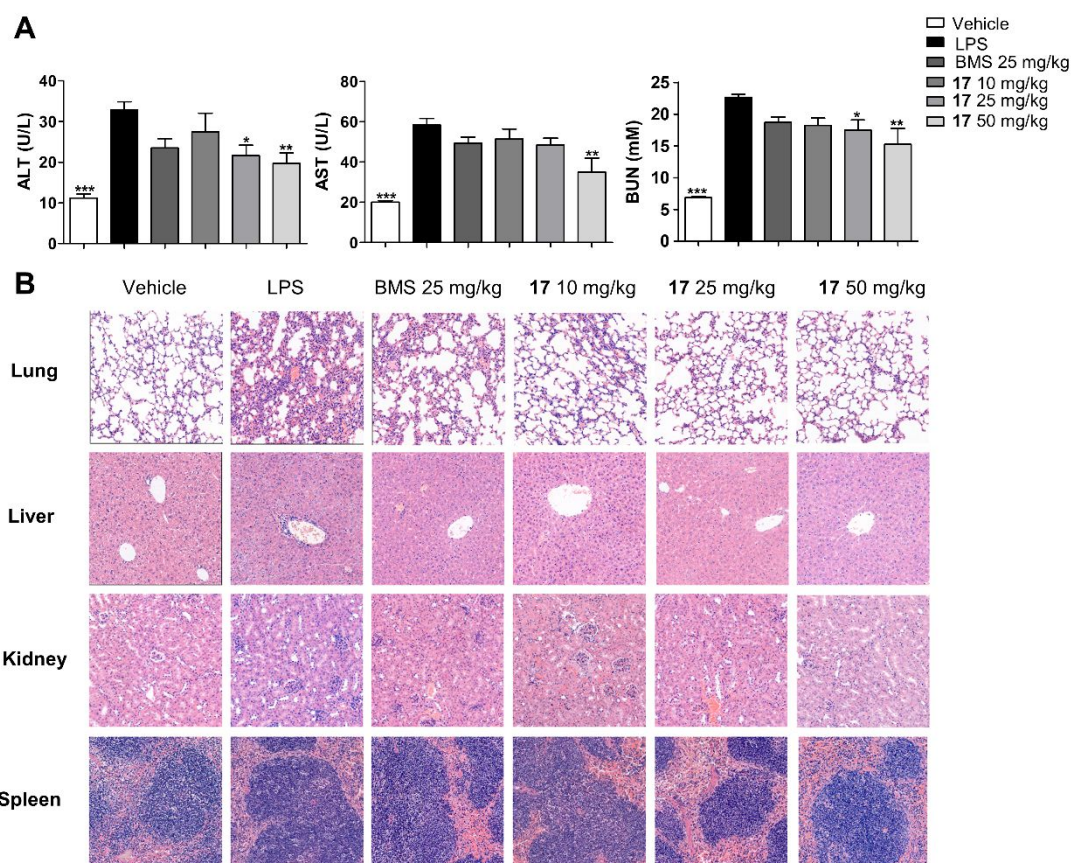
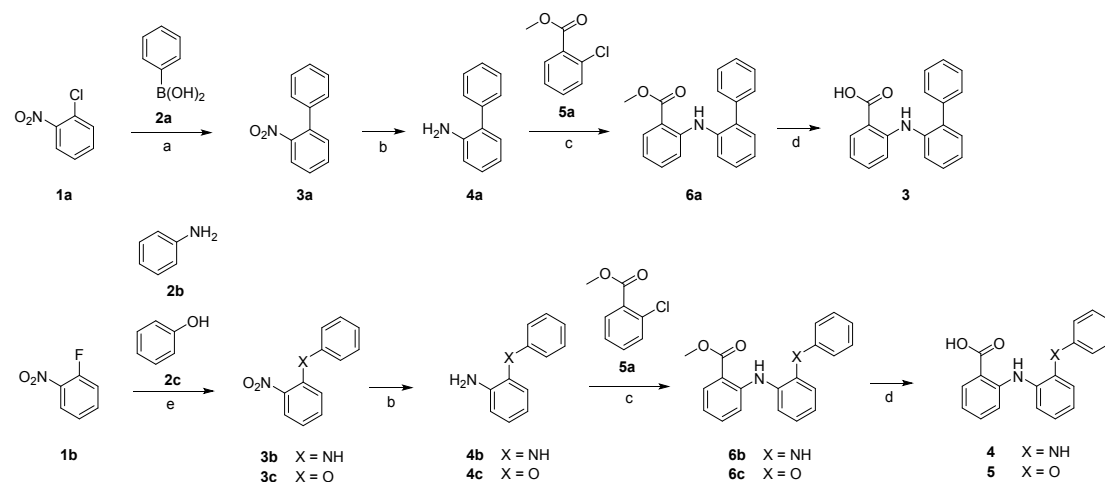


**Figure 8.** Compound **17** effectively protects mice from the LPS-induced multiorgan damage. (A) BMS309403 (25 mg/kg) or compound **17** (10, 25 and 50 mg/kg) administration decreases the level of tissue damage biomarkers ( $n = 8$  mice/group). (B) BMS309403 and compound **17** show an efficient protection against the LPS-induced injury in different organs. (H&E staining, magnification:  $\times 200$ ). Each image is representative of four mice at least. Data are given as mean  $\pm$  SEM and statistical analysis is performed by one-way ANOVA. \*  $P < 0.05$ , \*\*  $P < 0.01$ , \*\*\*  $P < 0.001$ , each vs LPS group.

**Chemistry.** The preparation of compounds **3-20** is depicted in Schemes 1-3. Commercially available compounds **1a** or **1c** were first coupled to the phenylboronic acid with different substituents by the Suzuki-Miyaura coupling reaction to yield compounds **3a** and **3d-3r**. In addition, compounds **3b** and **3c** were synthesized by a nucleophilic substitution reaction of aniline and phenol with 1-fluoro-2-nitrobenzene (**1b**). Compound **1j** was prepared by a methylation of 2,3-dichloro-4-nitroaniline (**1i**) using methyl iodide, and compound **1k** was a byproduct of this reaction. Compound **1l** was synthesized by a procedure similar to **1j**. Different nitrobenzene derivatives **3a-3s**

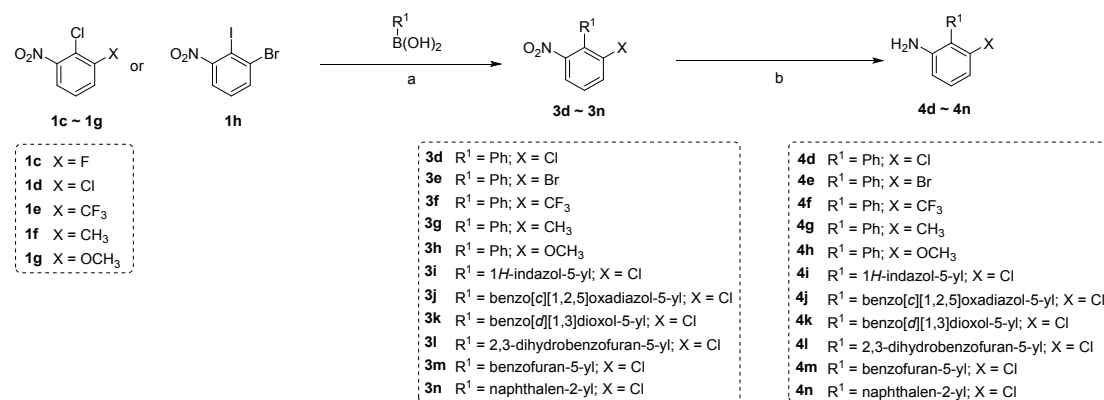
were then reduced by iron to afford the corresponding amines **4a-4r**. The target compounds were synthesized from these amines (**4a-4r**) by a palladium-catalyzed Buchwald-Hartwig amination followed by the hydrolysis of esters **6a-6r**.

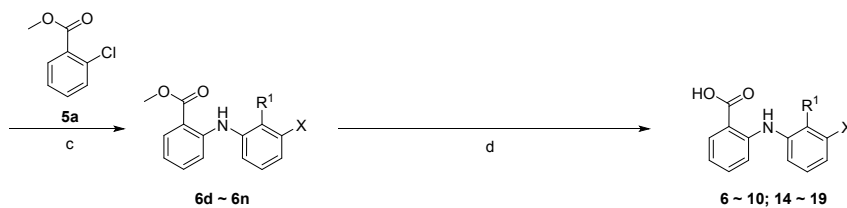
### Scheme 1. Synthesis of Compounds 3~5.



Reagents and conditions: (a) Pd(PPh<sub>3</sub>)<sub>4</sub>, K<sub>2</sub>CO<sub>3</sub>, dioxane, H<sub>2</sub>O, 15 h, 95 °C; (b) Fe, HAc, NH<sub>4</sub>Cl, EtOH, 50 °C; (c) Pd<sub>2</sub>(dba)<sub>3</sub>, BINAP, Cs<sub>2</sub>CO<sub>3</sub>, Toluene, 6 h, 90 °C; (d) NaOH, MeOH, H<sub>2</sub>O, 1 h, 70 °C; (e) NaH, THF, 2 h, 75 °C.

### Scheme 2. Synthesis of Compounds 6~10 and 14~19.

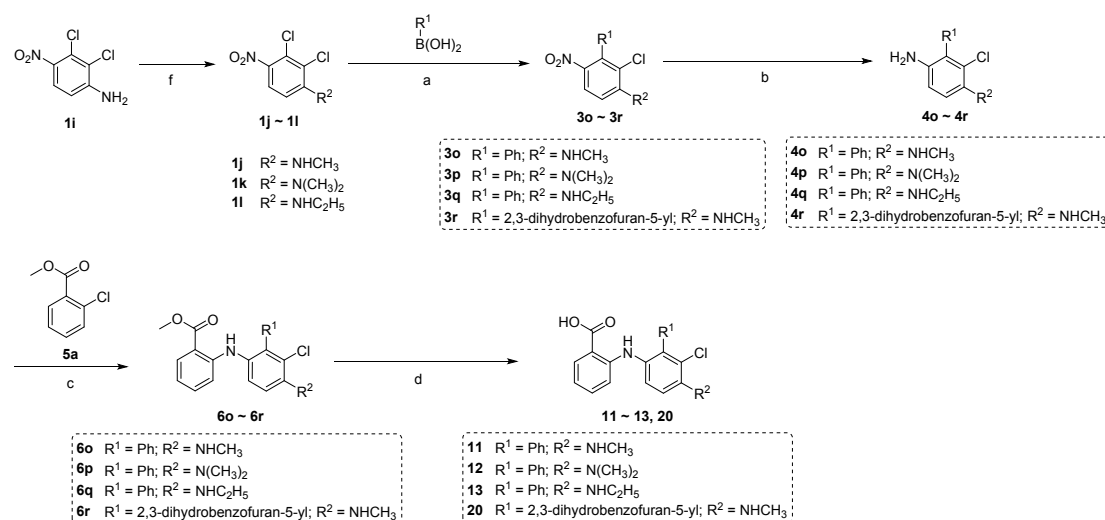




<b>6d</b> R <sup>1</sup> = Ph; X = Cl	<b>6j</b> R <sup>1</sup> = benzo[c][1,2,5]oxadiazol-5-yl; X = Cl	<b>6</b> R <sup>1</sup> = Ph; X = Cl	<b>14</b> R <sup>1</sup> = 1 <i>H</i> -indazol-5-yl; X = Cl
<b>6e</b> R <sup>1</sup> = Ph; X = Br	<b>6k</b> R <sup>1</sup> = benzo[d][1,3]dioxol-5-yl; X = Cl	<b>7</b> R <sup>1</sup> = Ph; X = Br	<b>15</b> R <sup>1</sup> = benzo[c][1,2,5]oxadiazol-5-yl; X = Cl
<b>6f</b> R <sup>1</sup> = Ph; X = CF <sub>3</sub>	<b>6l</b> R <sup>1</sup> = 2,3-dihydrobenzofuran-5-yl; X = Cl	<b>8</b> R <sup>1</sup> = Ph; X = CF <sub>3</sub>	<b>16</b> R <sup>1</sup> = benzo[d][1,3]dioxol-5-yl; X = Cl
<b>6g</b> R <sup>1</sup> = Ph; X = CH <sub>3</sub>	<b>6m</b> R <sup>1</sup> = benzofuran-5-yl; X = Cl	<b>9</b> R <sup>1</sup> = Ph; X = CH <sub>3</sub>	<b>17</b> R <sup>1</sup> = 2,3-dihydrobenzofuran-5-yl; X = Cl
<b>6h</b> R <sup>1</sup> = Ph; X = OCH <sub>3</sub>	<b>6n</b> R <sup>1</sup> = naphthalen-2-yl; X = Cl	<b>10</b> R <sup>1</sup> = Ph; X = OCH <sub>3</sub>	<b>18</b> R <sup>1</sup> = benzofuran-5-yl; X = Cl
<b>6i</b> R <sup>1</sup> = 1 <i>H</i> -indazol-5-yl; X = Cl			<b>19</b> R <sup>1</sup> = naphthalen-2-yl; X = Cl

Reagents and conditions: (a) Pd(PPh<sub>3</sub>)<sub>4</sub>, K<sub>2</sub>CO<sub>3</sub>, dioxane, H<sub>2</sub>O, 15 h, 95 °C; (b) Fe, HAc, NH<sub>4</sub>Cl, EtOH, 50 °C; (c) Pd<sub>2</sub>(dba)<sub>3</sub>, BINAP, Cs<sub>2</sub>CO<sub>3</sub>, Toluene, 6 h, 90 °C; (d) NaOH, MeOH, H<sub>2</sub>O, 1 h, 70 °C.

### Scheme 3. Synthesis of Compounds 11~13 and 20



Reagents and conditions: (a) Pd(PPh<sub>3</sub>)<sub>4</sub>, K<sub>2</sub>CO<sub>3</sub>, dioxane, H<sub>2</sub>O, 15 h, 95 °C; (b) Fe, HAc, NH<sub>4</sub>Cl, EtOH, 50 °C; (c) Pd<sub>2</sub>(dba)<sub>3</sub>, BINAP, Cs<sub>2</sub>CO<sub>3</sub>, Toluene, 6 h, 90 °C; (d) NaOH, MeOH, H<sub>2</sub>O, 1 h, 70 °C; (f) C<sub>2</sub>H<sub>5</sub>I or CH<sub>3</sub>I, CH<sub>3</sub>CN, 2 d, 85 °C.

## CONCLUSIONS

Here we reported the efficient discovery of a new class of highly potent, selective FABP4 inhibitors from an interesting fragment hit which displays multiple binding poses in the ligand binding pocket of FABP4. Both crystal structures and MD simulations revealed the multiple binding poses of the fragment. Based on three distinctive but partially overlapped binding poses of this fragment, compound **3** was

rationally designed, synthesized and evaluated, demonstrating a ~460-fold improvement in the binding affinity compared to the initial fragment. The binding affinity of compound **3** with FABP4 is superior to the well-known inhibitor, BMS309403. The protein-ligand structures determination together with the binding affinity precisely measured by ITC renders us to rapidly gain the sufficient knowledge of SAR and to discover more potent and selective FABP4 inhibitors. As a result, the representative compound (**17**) with a ~1300-fold improvement in the binding affinity compared to the initial fragment (**1**), is able to potently inhibit the production of MCP-1 and IL-6 in THP-1 macrophages as well as the lipolysis in 3T3-L1 adipocytes, with a better performance than BMS309403. Moreover, compound **17** displays favorable PK profiling for the *in vivo* study, and exhibits a better anti-inflammatory effect and effective protection against multi-organ damage in the LPS-induced inflammatory mice model compared to BMS309403. Given the good efficacy *in vivo*, application of **17** in other FABP4-associated indications such as breast cancer and non-alcoholic steatohepatitis will be explored in the future. Overall, the present study demonstrates that an in-depth exploration of fragment binding to the target protein plays a significant role in efficient discovery of novel and potent ligands. It is noteworthy that removing endogenous fatty acids from the purified FABP4 is crucial for elucidation of the multiple binding poses of the fragment, a weak binder, and for accurate determination of the binding affinity of highly potent FABP4 inhibitors by ITC.

## ■ EXPERIMENTAL SECTION

**Materials and Methods for Chemistry.** All chemical reagents and compounds included in our in-house library for screening were used as supplied by standard suppliers without further purification. All reactions were monitored by the thin-layer chromatography (TLC) and visualization was achieved by using ultraviolet light (254 nm). The column chromatography was carried out using a silica gel (300–400 mesh) in glass columns under proper pressure. <sup>1</sup>H NMR and <sup>13</sup>C NMR spectra were recorded on

a BRUKER AVANCE NEO 500 at 500 and 126 MHz, respectively. Coupling constants ( $J$ ) are expressed in hertz. Chemical shifts ( $\delta$ ) of NMR spectra are reported in parts per million (ppm) units. Mass spectra (MS) of compounds were measured using a Thermo Fisher FINNIGAN LTQ spectrometer. Purity of all compounds used for biological testing was determined to be > 95% by HPLC analysis. Analysis was performed on a SHIMADZU LC-20AD HPLC system under the following analytical method: column, SHIMADZU Shim-pack GIST C18 (5  $\mu$ m, 4.6 mm  $\times$  250 mm); solvent A: water containing 1% TFA; solvent B: acetonitrile; gradient, 60% B to 100% B over 15 min, 100% B for 5 min, 100% B to 60% B over 5 min; flow rate, 1 mL/min; detective wavelength, 254 nm; column temperature, 10  $^{\circ}$ C.

**Synthesis Procedure for 2-([1,1'-biphenyl]-2-ylamino)benzoic acid (**3**).** *2-Nitro-1,1'-biphenyl (3a)*. 1-chloro-2-nitrobenzene (**1a**) (0.1 g, 0.635 mmol), phenylboronic acid (**2a**) (0.077 g, 0.635 mmol), Pd(PPh<sub>3</sub>)<sub>4</sub> (0.059 g, 0.051 mmol) and K<sub>2</sub>CO<sub>3</sub> (0.263 g, 1.90 mmol) were taken up in 1,4-dioxane (8 mL) and water (2 mL) in a flask and purged with N<sub>2</sub> for 5 min. Then, the mixture was heat to 95  $^{\circ}$ C for 15 h. After cooling to room temperature, the mixture was filtered by celite and the filtrate was extracted with ethyl acetate, washed with brine, and the organic phase was dried over Na<sub>2</sub>SO<sub>4</sub>. The solvent was removed and the residue was purified by a flash column chromatography on silica (80% PE in ethyl acetate  $\sim$ 50% PE in ethyl acetate) to give a yellow solid **3a** (0.102 g, 80.67% yield). <sup>1</sup>H NMR (500 MHz, Chloroform-*d*)  $\delta$  7.63 – 7.58 (m, 4H), 7.44 (dd,  $J$  = 8.4, 7.0 Hz, 3H), 7.40 – 7.31 (m, 2H).

*[1,1'-Biphenyl]-2-amine (4a)*. Iron powder (561 mg, 10.04 mmol), NH<sub>4</sub>Cl (53.7 mg, 1.004 mmol) and AcOH (0.115 mL, 2.008 mmol) were added into water (2 ml) and stirred at 50  $^{\circ}$ C for 15 min. A solution of **3a** (200 mg, 1.004 mmol) in MeOH (3 ml) was added into the above solution quickly, and stirring was continued at 50  $^{\circ}$ C for 25 min. Then the reaction solution was alkalized to pH = 9 with an aqueous solution of sodium carbonate. The reaction mixture was filtered, the formed solid was washed with water and ethyl acetate. The combined filtrate was extracted with ethyl acetate. Then the combined organic layers were washed with brine, dried over anhydrous Na<sub>2</sub>SO<sub>4</sub>,

1  
2  
3  
4 filtered, and concentrated under reduced pressure to give the crude **4a** (180 mg), which  
5  
6 was directly used to the next step without further purification.

7  
8 *Methyl 2-([1,1'-biphenyl]-2-ylamino)benzoate (6a)*. Under nitrogen a solution of  
9  
10 Pd<sub>2</sub>(dba)<sub>3</sub> (14.23 mg, 0.016 mmol), BINAP (15.48 mg, 0.025 mmol) and [1,1'-  
11  
12 biphenyl]-2-amine (**4a**) (57.8 mg, 0.342 mmol) derivative in dry toluene (5 mL) was  
13  
14 stirred for 5 min. To this deep red solution, the corresponding methyl 2-chlorobenzoate  
15  
16 (53 mg, 0.311 mmol) and Cs<sub>2</sub>CO<sub>3</sub> (152 mg, 0.466 mmol) were added and stirring at 90  
17  
18 °C. The reaction was continued until the TLC showed the reaction to be completed  
19  
20 (usually 12 hours). The solid was filtered off and the filtrate concentrated in vacuo to  
21  
22 afford a residue that was subjected to a chromatography (silica gel, PM/EtOAc: 100/1-  
23  
24 10/1) to yield **6a**, methyl 2-([1,1'-biphenyl]-2-ylamino)benzoate (40 mg, 0.132 mmol,  
25  
26 42.4 % yield). <sup>1</sup>H NMR (500 MHz, DMSO-*d*<sub>6</sub>) δ 8.03 – 7.97 (m, 1H), 7.90 (dd, *J* = 7.5,  
27  
28 1.5 Hz, 1H), 7.65 (dd, *J* = 7.5, 1.6 Hz, 1H), 7.48 – 7.41 (m, 2H), 7.39 – 7.29 (m, 7H),  
29  
30 7.29 – 7.21 (m, 2H), 3.89 (s, 3H).

31  
32 *2-([1,1'-Biphenyl]-2-ylamino)benzoic acid (3)*. To a solution of **6a** (50 mg, 0.165  
33  
34 mmol) in methanol (4 mL) an aqueous solution of sodium hydroxide (5%, 4 mL) was  
35  
36 added and the reaction mixture was stirred for 1 h at 70 °C. After neutralization with  
37  
38 diluted hydrochloric acid (6 N), the solvents were removed and the product was washed  
39  
40 with water and dried to yield the corresponding acid (**3**, 44 mg, 0.152 mmol, 92% yield).  
41  
42 HPLC purity: 99.62% (RT = 12.11 min); ESI-MS: 288.5 [M-H]<sup>-</sup>, 599.4 [2M-H+Na]<sup>-</sup>;  
43  
44 <sup>1</sup>H NMR (500 MHz, DMSO-*d*<sub>6</sub>) δ 12.83 (s, 1H), 9.56 (s, 1H), 7.82 (dd, *J* = 7.9, 1.7 Hz,  
45  
46 1H), 7.48 (dd, *J* = 8.1, 1.3 Hz, 1H), 7.41 – 7.30 (m, 8H), 7.22 (td, *J* = 7.4, 1.3 Hz, 1H),  
47  
48 7.11 (dd, *J* = 8.5, 1.1 Hz, 1H), 6.73 – 6.70 (m, 1H); <sup>13</sup>C NMR (126 MHz, Methanol-*d*<sub>4</sub>)  
49  
50 δ 170.14, 148.36, 139.27, 137.80, 136.66, 133.58, 131.76, 130.80, 128.68, 127.98,  
51  
52 127.82, 126.87, 124.16, 123.94, 116.42, 113.28, 112.04.

53  
54 **Synthesis Procedure for 2-((2-(phenylamino)phenyl)amino)benzoic acid (4)**. *2-*  
55  
56 *nitro-N-phenylaniline (3b)*. To a solution of NaH (170 mg, 4.25 mmol) (60 percent  
57  
58 dispersion in mineral oil) in THF (8 mL) was slowly added aniline (198 mg, 2.126  
59  
60 mmol). After 15 minutes of stirring, 1-fluoro-2-nitrobenzene (300 mg, 2.126 mmol)

1  
2  
3  
4 was added and the resulting solution was heated to 75 °C for 1 hour. The reaction  
5  
6 mixture was cooled to room temperature, quenched with water (5 mL) and extracted  
7  
8 with EtOAc. The combined organic phases were washed with brine (5 mL), dried over  
9  
10 Na<sub>2</sub>SO<sub>4</sub> and concentrated. The crude residue was purified by the flash chromatography  
11  
12 (eluent: EtOAc/PE = 50/1) to give the desired product, 2-nitro-*N*-phenylaniline (**3b**,  
13  
14 430 mg, 2.007 mmol, 94 % yield). <sup>1</sup>H NMR (500 MHz, DMSO-*d*<sub>6</sub>) δ 9.42 (s, 1H), 8.15  
15  
16 (dd, *J* = 7.5, 1.5 Hz, 1H), 7.39 – 7.35 (m, 1H), 7.32 – 7.25 (m, 2H), 7.24 – 7.21 (m, 2H),  
17  
18 7.19 – 7.16 (m, 1H), 7.02 – 6.98 (m, 1H), 6.90 (dd, *J* = 7.5, 1.5 Hz, 1H).

19  
20 Compounds **4b**, **6b** and **4** were prepared following the synthetic procedure similar  
21  
22 to that of compounds **4a**, **6a** and **3**, respectively. 2-((2-  
23  
24 (phenylamino)phenyl)amino)benzoic acid (**4**, white powder, 32 mg, 72 % yield for the  
25  
26 last step). HPLC purity: 95.13% (RT = 11.73 min); ESI-MS: 303.6 [M-H]<sup>-</sup>, 629.4  
27  
28 [2M-H+Na]<sup>-</sup>; <sup>1</sup>H NMR (500 MHz, DMSO-*d*<sub>6</sub>) δ 12.85 (s, 1H), 9.43 (s, 1H), 7.86 (dd, *J*  
29  
30 = 8.0, 1.7 Hz, 1H), 7.57 (s, 1H), 7.38 – 7.33 (m, 2H), 7.27 – 7.25 (m, 1H), 7.13 (t, *J*  
31  
32 = 7.8 Hz, 2H), 7.10 – 6.99 (m, 3H), 6.89 (d, *J* = 8.0 Hz, 2H), 6.76 – 6.71 (m, 2H); <sup>13</sup>C  
33  
34 NMR (126 MHz, DMSO-*d*<sub>6</sub>) δ 170.16, 147.98, 145.01, 137.00, 134.38, 133.04, 132.17,  
35  
36 129.35, 124.60, 123.15, 122.75, 121.15, 119.63, 117.28, 116.83, 114.04, 113.15.

37  
38 **2-((2-Phenoxyphenyl)amino)benzoic acid (5)**. The title compound (white powder,  
39  
40 23 mg, 92% yield for the last step) was prepared analogous to compound **4**. HPLC  
41  
42 purity: 99.03% (RT = 9.47 min); ESI-MS: 304.5 [M-H]<sup>-</sup>, 631.4 [2M-H+Na]<sup>-</sup>; <sup>1</sup>H NMR  
43  
44 (500 MHz, DMSO-*d*<sub>6</sub>) δ 12.41 (s, 1H), 9.82 (s, 1H), 7.85 (dd, *J* = 7.9, 1.5 Hz, 1H), 7.59  
45  
46 – 7.57 (m, 1H), 7.43 – 7.40 (m, 1H), 7.33 – 7.29 (m, 3H), 7.23 – 7.19 (m, 1H), 7.11 –  
47  
48 7.05 (m, 3H), 6.92 (d, *J* = 8.0 Hz, 2H), 6.79 (t, *J* = 7.5 Hz, 1H); <sup>13</sup>C NMR (126 MHz,  
49  
50 DMSO-*d*<sub>6</sub>) δ 170.26, 157.53, 147.54, 146.59, 134.50, 133.19, 132.23, 130.34, 125.29,  
51  
52 123.98, 123.40, 121.64, 121.30, 118.19, 117.45, 114.32, 113.73.

53  
54 **2-((6-chloro-[1,1'-biphenyl]-2-yl)amino)benzoic acid (6)**. The title compound  
55  
56 (white powder, 40 mg, 92% yield for the last step) was prepared analogous to  
57  
58 compound **3**. HPLC purity: 97.68% (RT = 19.46 min); ESI-MS: 322.1 [M-H]<sup>-</sup>, 667.1  
59  
60 [2M-H+Na]<sup>-</sup>; <sup>1</sup>H NMR (500 MHz, DMSO-*d*<sub>6</sub>) δ 10.40 (s, 1H), 7.81 (dd, *J* = 7.7, 1.7 Hz,

1  
2  
3  
4 1H), 7.43 (t,  $J = 7.4$  Hz, 3H), 7.37 – 7.35 (m, 1H), 7.29 (t,  $J = 8.1$  Hz, 1H), 7.26 – 7.20  
5 (m, 3H), 7.18 (d,  $J = 8.0$  Hz, 1H), 7.13 (d,  $J = 8.0$  Hz, 1H), 6.72 – 6.69 (m, 1H);  $^{13}\text{C}$   
6 NMR (126 MHz, DMSO- $d_6$ )  $\delta$  169.43, 145.98, 140.53, 135.47, 134.04, 133.43, 132.95,  
7 131.64, 129.54, 129.25, 128.68, 127.99, 123.33, 118.86, 118.06, 114.19, 113.21.

8  
9  
10  
11 **2-((6-bromo-[1,1'-biphenyl]-2-yl)amino)benzoic acid (7)**. The title compound  
12 (white powder, 31 mg, 91% yield for the last step) was prepared analogous to  
13 compound **3**. HPLC purity: 96.18% (RT = 13.38 min); ESI-MS: 366.2 [M-H] $^-$ , 734.2  
14 [2M-H] $^-$ ;  $^1\text{H}$  NMR (500 MHz, DMSO- $d_6$ )  $\delta$  9.21 (s, 1H), 7.78 (dd,  $J = 7.9, 1.8$  Hz, 1H),  
15 7.53 (dd,  $J = 8.1, 0.8$  Hz, 1H), 7.47 – 7.37 (m, 5H), 7.32 – 7.28 (m, 2H), 7.22 – 7.20  
16 (m, 2H), 6.80 – 6.77 (m, 1H);  $^{13}\text{C}$  NMR (126 MHz, DMSO- $d_6$ )  $\delta$  169.95, 146.42, 141.03,  
17 137.97, 135.31, 134.39, 132.12, 130.11, 129.90, 129.15, 128.45, 126.87, 124.52,  
18 119.79, 118.53, 114.64, 113.99.

19  
20  
21  
22 **2-((6-(trifluoromethyl)-[1,1'-biphenyl]-2-yl)amino)benzoic acid (8)**. The title  
23 compound (white powder, 10 mg, 82% yield for the last step) was prepared analogous  
24 to compound **3**. HPLC purity: 96.62% (RT = 13.03 min); ESI-MS: 356.2 [M-H] $^-$ ,  
25 712.5 [2M-H] $^-$ ;  $^1\text{H}$  NMR (500 MHz, DMSO- $d_6$ )  $\delta$  12.98 (s, 1H), 9.11 (s, 1H), 7.84 –  
26 7.76 (m, 2H), 7.58 (t,  $J = 8.0$  Hz, 1H), 7.51 – 7.49 (m, 1H), 7.46 – 7.40 (m, 4H), 7.30  
27 (dd,  $J = 8.5, 1.1$  Hz, 1H), 7.24 – 7.22 (m, 2H), 6.82 – 6.79 (m, 1H);  $^{13}\text{C}$  NMR (126  
28 MHz, DMSO- $d_6$ )  $\delta$  169.87, 146.18, 141.17, 135.02, 134.53, 132.99, 132.89, 132.16,  
29 129.98, 129.22, 128.81, 128.61, 124.11, 119.96, 119.92, 118.79, 114.55, 113.95.

30  
31  
32  
33 **2-((6-methyl-[1,1'-biphenyl]-2-yl)amino)benzoic acid (9)**. The title compound  
34 (white powder, 30 mg, 87% yield for the last step) was prepared analogous to  
35 compound **3**. HPLC purity: 99.45% (RT = 13.33 min); ESI-MS: 302.2 [M-H] $^-$ , 604.6  
36 [2M-H] $^-$ ;  $^1\text{H}$  NMR (500 MHz, DMSO- $d_6$ )  $\delta$  9.11 (s, 1H), 7.76 (dd,  $J = 7.9, 1.8$  Hz, 1H),  
37 7.42 (t,  $J = 7.5$  Hz, 2H), 7.36 – 7.32 (m, 3H), 7.27 (t,  $J = 7.7$  Hz, 1H), 7.21 – 7.16 (m,  
38 3H), 7.05 (d,  $J = 7.4$  Hz, 1H), 6.71 – 6.68 (m, 1H), 2.02 (s, 3H);  $^{13}\text{C}$  NMR (126 MHz,  
39 DMSO- $d_6$ )  $\delta$  169.99, 147.69, 138.77, 138.01, 137.53, 135.55, 134.44, 132.11, 129.73,  
40 129.13, 128.14, 127.74, 125.31, 119.35, 117.42, 114.02, 112.72, 21.04.

41  
42  
43  
44  
45  
46  
47  
48  
49  
50  
51  
52  
53  
54  
55  
56  
57  
58 **2-((6-methoxy-[1,1'-biphenyl]-2-yl)amino)benzoic acid (10)**. The title compound

(white powder, 41 mg, 91% yield for the last step) was prepared analogous to compound **3**. HPLC purity: 95.15% (RT = 10.32 min); ESI-MS: 318.3 [M-H]<sup>-</sup>; <sup>1</sup>H NMR (500 MHz, DMSO-*d*<sub>6</sub>) δ 12.84 (s, 1H), 9.19 (s, 1H), 7.77 (dd, *J* = 7.9, 1.7 Hz, 1H), 7.38 – 7.27 (m, 5H), 7.23 – 7.17 (m, 3H), 7.11 (d, *J* = 7.8 Hz, 1H), 6.86 (d, *J* = 8.2 Hz, 1H), 6.73 – 6.70 (m, 1H), 3.69 (s, 3H); <sup>13</sup>C NMR (126 MHz, DMSO-*d*<sub>6</sub>) δ 170.02, 158.04, 147.47, 139.75, 135.03, 134.39, 132.11, 130.66, 129.14, 128.66, 127.55, 124.12, 117.64, 114.36, 114.31, 113.09, 106.80, 56.07.

**Synthesis Procedure for 2-((6-chloro-5-(methylamino)-[1,1'-biphenyl]-2-yl)amino)benzoic acid (11).** 2,3-dichloro-*N*-methyl-4-nitroaniline (**1j**) and 2,3-dichloro-*N,N*-dimethyl-4-nitroaniline (**1k**). The mixture of 2,3-dichloro-4-nitroaniline (1.2 g, 5.80 mmol), iodomethane (11.55 mL, 185 mmol), K<sub>2</sub>CO<sub>3</sub> (2.403 g, 17.39 mmol), and CH<sub>3</sub>CN (30 mL) was refluxed for 3 days. The solvent was removed and added with water. The solution was extracted with dichloromethane, and dried with Na<sub>2</sub>SO<sub>4</sub>. After solvent removal, the crude material was subject to a column chromatography (silica, EtOAc/PE = 1/8) to give 2,3-dichloro-*N*-methyl-4-nitroaniline (**1j**, yellow powder, 800 mg, 3.62 mmol, 62.4% yield) as a primary product and 2,3-dichloro-*N,N*-dimethyl-4-nitroaniline (**1k**, yellow powder, 50 mg, 0.213 mmol, 3.67% yield) as a byproduct. For **1j**, <sup>1</sup>H NMR (500 MHz, Chloroform-*d*) δ 7.93 (d, *J* = 9.3 Hz, 1H), 6.49 (d, *J* = 9.3 Hz, 1H), 5.13 (s, 1H), 2.95 (d, *J* = 5.1 Hz, 3H). For **1k**, <sup>1</sup>H NMR (500 MHz, Chloroform-*d*) δ 7.81 (d, *J* = 9.1 Hz, 1H), 6.94 (d, *J* = 9.1 Hz, 1H), 2.96 (s, 6H).

Compounds **3o**, **4o**, **6o** and **11** were prepared following the synthetic procedure similar to that of compounds **3a**, **4a**, **6a** and **3**, respectively. 2-((6-chloro-5-(methylamino)-[1,1'-biphenyl]-2-yl)amino)benzoic acid (**11**). Yellow powder, 40 mg, 69% yield for the last step. HPLC purity: 97.50% (RT = 10.62 min); ESI-MS: 351.0 [M-H]<sup>-</sup>; <sup>1</sup>H NMR (500 MHz, DMSO-*d*<sub>6</sub>) δ 12.67 (s, 1H), 8.93 (s, 1H), 7.68 (dd, *J* = 8.0, 1.7 Hz, 1H), 7.35 – 7.24 (m, 5H), 7.13 – 7.12 (m, 2H), 6.77 – 6.73 (m, 2H), 6.57 (t, *J* = 7.4 Hz, 1H), 5.56 (q, *J* = 5.0 Hz, 1H), 2.83 (d, *J* = 4.6 Hz, 3H); <sup>13</sup>C NMR (126 MHz, DMSO-*d*<sub>6</sub>) δ 170.21, 149.94, 143.50, 138.54, 137.81, 137.39, 133.58, 131.96, 129.69, 128.48, 127.78, 125.87, 117.92, 115.88, 113.05, 110.30, 30.67.

**Synthesis Procedure for 2-((6-chloro-5-(dimethylamino)-[1,1'-biphenyl]-2-yl)amino)benzoic acid (12).** Compound **12** was synthesized from the byproduct **1k**, and the preparation of **12** was similar to that of compound **3**. Light yellow powder, 8 mg, 82% yield for the last step. HPLC purity: 99.60% (RT = 3.31 min); ESI-MS: 365.3 [M-H]<sup>-</sup>, 729.5 [2M-H]<sup>-</sup>; <sup>1</sup>H NMR (500 MHz, DMSO-*d*<sub>6</sub>) δ 12.80 (s, 1H), 9.06 (s, 1H), 7.74 (dd, *J* = 7.9, 1.7 Hz, 1H), 7.43 – 7.39 (m, 3H), 7.36 – 7.32 (m, 2H), 7.25 (d, *J* = 8.8 Hz, 1H), 7.18 – 7.17 (m, 2H), 7.08 (d, *J* = 8.4 Hz, 1H), 6.70 – 6.67 (m, 1H), 2.74 (s, 6H); <sup>13</sup>C NMR (126 MHz, DMSO-*d*<sub>6</sub>) δ 169.95, 147.85, 136.85, 136.54, 135.06, 134.60, 134.55, 132.06, 129.83, 128.94, 128.35, 128.19, 121.99, 120.42, 117.50, 113.83, 112.49, 44.30.

**2-((6-chloro-5-(ethylamino)-[1,1'-biphenyl]-2-yl)amino)benzoic acid (13).** The title compound (light yellow powder, 18 mg, 67% yield for the last step) was prepared analogous to compound **11**. HPLC purity: 98.25% (RT = 8.97 min); ESI-MS: 365.2 [M-H]<sup>-</sup>; <sup>1</sup>H NMR (500 MHz, DMSO-*d*<sub>6</sub>) δ 12.66 (s, 1H), 8.92 (s, 1H), 7.98 (dd, *J* = 7.9, 1.1 Hz, 1H), 7.72 – 7.68 (m, 2H), 7.48 (td, *J* = 7.6, 1.2 Hz, 1H), 7.35 – 7.32 (m, 1H), 7.30 – 7.27 (m, 1H), 7.26 – 7.21 (m, 2H), 7.14 – 7.12 (m, 1H), 6.80 – 6.76 (m, 1H), 6.59 – 6.56 (m, 1H), 5.24 (s, 1H), 3.23 (q, *J* = 7.1 Hz, 2H), 1.22 (t, *J* = 7.1 Hz, 3H); <sup>13</sup>C NMR (126 MHz, DMSO-*d*<sub>6</sub>) δ 170.24, 149.99, 142.45, 137.95, 137.34, 134.01, 131.94, 130.12, 129.63, 128.52, 128.10, 127.83, 125.93, 118.04, 116.03, 113.13, 110.76, 38.02, 14.90.

**2-((3-chloro-2-(1*H*-indazol-5-yl)phenyl)amino)benzoic acid (14).** The title compound (white powder, 12 mg, 76% yield for the last step) was prepared analogous to compound **3**. HPLC purity: 97.93% (RT = 8.67 min); ESI-MS: 362.3 [M-H]<sup>-</sup>, 724.8 [2M-H]<sup>-</sup>; <sup>1</sup>H NMR (500 MHz, DMSO-*d*<sub>6</sub>) δ 12.98 (s, 2H), 9.27 (s, 1H), 8.09 (s, 1H), 7.75 (dd, *J* = 7.9, 1.7 Hz, 1H), 7.65 (s, 1H), 7.60 (d, *J* = 8.5 Hz, 1H), 7.52 – 7.51 (m, 1H), 7.43 – 7.34 (m, 3H), 7.26 – 7.24 (m, 1H), 7.15 (dd, *J* = 8.5, 1.6 Hz, 1H), 6.78 – 6.75 (m, 1H). <sup>13</sup>C NMR (125 MHz, DMSO-*d*<sub>6</sub>) δ 169.50, 153.91, 146.46, 145.84, 140.90, 134.14, 133.90, 132.80, 131.70, 130.14, 129.23, 127.70, 125.97, 123.10, 122.54, 118.33, 118.13, 114.15, 113.22, 111.72.

**2-((2-(benzo[*c*][1,2,5]oxadiazol-5-yl)-3-chlorophenyl)amino)benzoic acid (15).**

The title compound (light yellow powder, 16 mg, 66% yield for the last step) was prepared analogous to compound **3**. HPLC purity: 98.95% (RT = 13.05 min); ESI-MS: 364.0 [M-H]<sup>-</sup>; <sup>1</sup>H NMR (500 MHz, DMSO-*d*<sub>6</sub>) δ 12.95 (s, 1H), 9.50 (s, 1H), 8.15-8.11 (m, 2H), 7.77 (dd, *J* = 7.9, 1.4 Hz, 1H), 7.59 (d, *J* = 8.2 Hz, 1H), 7.50 – 7.42 (m, 3H), 7.36-7.31 (m, 2H), 6.82 – 6.79 (m, 1H); <sup>13</sup>C NMR (126 MHz, DMSO-*d*<sub>6</sub>) δ 170.22, 149.45, 148.71, 146.16, 141.02, 140.45, 135.89, 134.67, 133.35, 132.13, 131.14, 130.93, 124.03, 119.69, 118.91, 117.96, 117.09, 114.73, 113.73.

**2-((2-(benzo[*d*][1,3]dioxol-5-yl)-3-chlorophenyl)amino)benzoic acid (16).** The title compound (white powder, 35 mg, 86% yield for the last step) was prepared analogous to compound **3**. HPLC purity: 99.68% (RT = 12.59 min); ESI-MS: 366.0 [M-H]<sup>-</sup>; <sup>1</sup>H NMR (500 MHz, DMSO-*d*<sub>6</sub>) δ 13.08 (s, 1H), 9.37 (s, 1H), 7.87 (dd, *J* = 8.0, 1.7 Hz, 1H), 7.54 (dd, *J* = 8.1, 1.0 Hz, 1H), 7.47 (ddd, *J* = 8.7, 7.0, 1.8 Hz, 1H), 7.42 – 7.36 (m, 2H), 7.28 (dd, *J* = 8.0, 1.1 Hz, 1H), 7.04 (d, *J* = 7.9 Hz, 1H), 6.87 – 6.84 (m, 2H), 6.75 (dd, *J* = 7.9, 1.8 Hz, 1H), 6.11 (d, *J* = 7.8 Hz, 2H); <sup>13</sup>C NMR (126 MHz, DMSO-*d*<sub>6</sub>) δ 170.15, 147.92, 147.34, 146.19, 141.62, 134.32, 134.10, 132.70, 132.18, 129.58, 129.47, 123.69, 123.32, 118.59, 118.55, 114.76, 110.49, 109.13, 108.81, 101.56.

**2-((3-chloro-2-(2,3-dihydrobenzofuran-5-yl)phenyl)amino)benzoic acid (17).**

The title compound (light yellow powder, 5.5 g, 81% yield for the last step) was prepared analogous to compound **3**. HPLC purity: 99.22% (RT = 13.06 min); ESI-MS: 364.0 [M-H]<sup>-</sup>; <sup>1</sup>H NMR (500 MHz, DMSO-*d*<sub>6</sub>) δ 9.62 (s, 1H), 7.82 (dd, *J* = 7.8, 1.7 Hz, 1H), 7.45 (dd, *J* = 8.2, 1.1 Hz, 1H), 7.36 – 7.26 (m, 3H), 7.18 (dd, *J* = 8.0, 1.1 Hz, 1H), 7.08 (d, *J* = 1.8 Hz, 1H), 6.93 (dd, *J* = 8.1, 1.9 Hz, 1H), 6.82 – 6.75 (m, 2H), 4.55 (t, *J* = 8.8 Hz, 2H), 3.21 – 3.16 (m, 2H); <sup>13</sup>C NMR (126 MHz, DMSO-*d*<sub>6</sub>) δ 169.94, 159.85, 146.37, 141.39, 134.52, 134.42, 133.23, 132.19, 129.79, 129.36, 128.17, 127.67, 126.79, 123.57, 118.82, 118.57, 114.75, 113.86, 109.58, 71.48, 29.49.

**2-((2-(benzofuran-5-yl)-3-chlorophenyl)amino)benzoic acid (18).** The title compound (white powder, 18 mg, 91% yield for the last step) was prepared analogous

1  
2  
3  
4 to compound **3**. HPLC purity: 98.02% (RT = 13.48 min); ESI-MS: 362.1 [M-H]<sup>-</sup>; <sup>1</sup>H  
5 NMR (500 MHz, DMSO-*d*<sub>6</sub>) δ 12.91 (s, 1H), 9.26 (s, 1H), 8.03 (d, *J* = 2.2 Hz, 1H),  
6 7.77 (dd, *J* = 7.9, 1.7 Hz, 1H), 7.67 (d, *J* = 8.4 Hz, 1H), 7.55 – 7.52 (m, 2H), 7.44 – 7.35  
7 (m, 3H), 7.27 – 7.26 (m, 1H), 7.15 (dd, *J* = 8.5, 1.8 Hz, 1H), 6.98 (dd, *J* = 2.1, 0.7 Hz,  
8 1H), 6.80 – 6.77 (m, 1H); <sup>13</sup>C NMR (151 MHz, DMSO-*d*<sub>6</sub>) δ 169.88, 154.30, 146.85,  
9 146.23, 141.28, 134.52, 134.28, 133.19, 132.09, 130.53, 129.61, 128.09, 126.36,  
10 123.49, 122.93, 118.72, 118.52, 114.54, 113.61, 112.10, 107.39.

11  
12  
13  
14  
15  
16  
17 **2-((3-chloro-2-(naphthalen-2-yl)phenyl)amino)benzoic acid (19)**. The title  
18 compound (white powder, 41 mg, 86% yield for the last step) was prepared analogous  
19 to compound **3**. HPLC purity: 95.05% (RT = 14.77 min); ESI-MS: 372.1 [M-H]<sup>-</sup>; <sup>1</sup>H  
20 NMR (500 MHz, DMSO-*d*<sub>6</sub>) δ 12.83 (s, 1H), 9.44 (s, 1H), 8.05 – 8.00 (m, 3H), 7.92 (s,  
21 1H), 7.81 (dd, *J* = 8.0, 1.7 Hz, 1H), 7.63 – 7.58 (m, 3H), 7.48 (t, *J* = 8.1 Hz, 2H), 7.42  
22 – 7.39 (m, 2H), 7.36 – 7.34 (m, 1H), 6.85 – 6.82 (m, 1H); <sup>13</sup>C NMR (126 MHz, DMSO-  
23 *d*<sub>6</sub>) δ 170.10, 146.34, 141.01, 134.85, 134.59, 133.83, 133.32, 132.15, 132.11, 130.11,  
24 129.29, 123.82, 119.30, 118.66, 114.61, 113.67.

25  
26  
27  
28  
29  
30  
31  
32  
33 **2-((3-chloro-2-(2,3-dihydrobenzofuran-5-yl)-4-(methylamino)phenyl)amino)**  
34 **benzoic acid (20)**. The title compound (light yellow powder, 12 mg, 78% yield for the  
35 last step) was prepared analogous to compound **11**. HPLC purity: 98.19% (RT = 10.07  
36 min); ESI-MS: 393.4 [M-H]<sup>-</sup>; <sup>1</sup>H NMR (500 MHz, DMSO-*d*<sub>6</sub>) δ 12.67 (s, 1H), 8.94 (s,  
37 1H), 7.71 (dd, *J* = 8.0, 1.7 Hz, 1H), 7.28 – 7.23 (m, 2H), 6.96 (d, *J* = 1.8 Hz, 1H), 6.83  
38 – 6.79 (m, 2H), 6.70 (d, *J* = 8.4 Hz, 2H), 6.60 – 6.57 (m, 1H), 5.51 (q, *J* = 4.6 Hz, 1H),  
39 4.51 (t, *J* = 8.8 Hz, 2H), 3.20 – 3.14 (m, 1H), 3.09 – 3.03 (m, 1H), 2.82 (d, *J* = 4.8 Hz,  
40 3H); <sup>13</sup>C NMR (126 MHz, DMSO-*d*<sub>6</sub>) δ 170.10, 159.38, 150.16, 143.61, 137.68, 134.42,  
41 134.36, 131.94, 129.34, 129.07, 128.21, 127.39, 126.44, 125.73, 118.43, 116.14,  
42 113.27, 109.89, 108.96, 71.33, 30.66, 29.48.

43  
44  
45  
46  
47  
48  
49  
50  
51  
52  
53 **Protein Expression and Purification.** The cDNA of full length FABP3, FABP4  
54 and FABP5 were cloned into the PET28a vector with an N-terminal 6His tag. The  
55 plasmid was then transformed into BL21 (DE3) cells for protein expression. The  
56 expressed protein was purified by a Ni-NTA column (GE) followed by a size exclusion  
57  
58  
59

1  
2  
3  
4 chromatography (Superdex200, GE Healthcare). The purified FABP3, FABP4 and  
5  
6 FABP5 were stored in a solution (50 mM NaCl, 20 mM HEPES, pH 7.5). To obtain  
7  
8 apo FABP3, apo FABP4 and apo FABP5, purified FABP3, FABP4 and FABP5 were  
9  
10 delipidated as previously reported.<sup>38</sup> Briefly, the protein was concentrated to 10 mg/ml.  
11  
12 For each 1 mL protein, 3.75 mL mixture of chloroform and methanol (1:2) was added.  
13  
14 After thoroughly vortexing, 1.25 mL chloroform was added followed by another  
15  
16 mixing step. Afterwards, 1.25 mL distilled water was added and vortexed well. The  
17  
18 suspension was centrifuged at 1000 rpm for 5 min at room temperature to give two-  
19  
20 phase system. The precipitated protein at the bottom was denatured in a buffer  
21  
22 containing 50 mM Tris-HCl (pH 8.0), 6 M guanidinium chloride, and 2 mM DTT, and  
23  
24 refolded by a fast dilution at 4 °C in 250 mL buffer composed of 20 mM Tris-HCl (pH  
25  
26 8.5), 1.7 M urea, 4% glycerol, and 2 mM DTT. Then the concentration of urea in the  
27  
28 buffer was adjusted to 2 M with addition of 8 M urea. Refolded protein was  
29  
30 concentrated and dialyzed against PBS at 4 °C overnight followed by a further  
31  
32 purification via the size exclusion chromatography (Superdex200, GE Healthcare).

33 **Protein Crystallization and Structure Determination.** The purified FABP4  
34  
35 protein was concentrated to 5 mg/mL for crystallization. Crystals of apo FABP4 were  
36  
37 obtained at 20 °C by mixing equal volumes of FABP4 and reservoir (1.6 M trisodium  
38  
39 citrate, pH 6.5 or 7.5) with a hanging-drop vapor diffusion method. Complex crystals  
40  
41 were obtained by soaking apo crystals into the reservoir solution containing 2–10 mM  
42  
43 of compounds overnight. Crystals were flash frozen in liquid nitrogen in the presence  
44  
45 of the reservoir solution supplemented with 20% ethylene glycol. X-ray diffraction data  
46  
47 were collected at beamline BL17U1, BL18U1 or BL19U1 at the Shanghai Synchrotron  
48  
49 Radiation Facility.<sup>39</sup> The data were processed with HKL3000 software packages.<sup>40</sup> The  
50  
51 complex structures were solved by molecular replacement using the program  
52  
53 PHASER<sup>41</sup> with a search model of PDB code 4NNT.<sup>26</sup> The models were built using  
54  
55 COOT<sup>42</sup> and refined with a simulated-annealing protocol implemented in the program  
56  
57 PHENIX.<sup>43</sup> The refined structures were deposited to Protein Data Bank with accession  
58  
59 codes listed in Table S1 in Supporting Information. The complete statistics as well as  
60

1  
2  
3  
4 the quality of solved structures are also shown in Table S1.

5  
6 **1,8-ANS (8-anilino-1-naphthalene-sulfonic acid) Displacement Assay.** The 1,8-  
7  
8 ANS displacement assay developed by Kurian *et al.*<sup>44</sup> was used to determine binding  
9  
10 affinities of compounds with FABP4, FABP5 or FABP3. Briefly, compounds at various  
11  
12 concentrations were incubated in the 96-well plate in dark with the recombinant apo  
13  
14 FABP4, apo FABP5 or apo FABP3 for 10 min. Next, 10  $\mu\text{M}$  1,8-ANS was added and  
15  
16 incubated for another 3 min at room temperature in dark. The fluorescence signal at  
17  
18 370 nm (excitation)/470 nm (emission) was measured with Bio-Tek Synergy4 plate  
19  
20 reader. It was reported that 1,8-ANS is sensitive to light and slight differences in the  
21  
22 amount of co-solvent in the assay.<sup>20</sup> To deal with this, 2 mM 1,8-ANS in DMSO was  
23  
24 divided into 100  $\mu\text{L}$ /tube and stored at  $-80\text{ }^\circ\text{C}$  in dark. In addition, inhibition ratios of  
25  
26 BMS309403 at three concentrations (0.5  $\mu\text{M}$ , 1  $\mu\text{M}$  and 2  $\mu\text{M}$ ) were tested as a control  
27  
28 for each 96-well plate. For each compound, at least three independent experiments were  
29  
30 performed for the determination of  $\text{IC}_{50}$ . All experimental data were analyzed using  
31  
32 GraphPad Prism, version 8.0 (GraphPad Inc.).  $K_i$  values were calculated according to  
33  
34 the equation  $K_i = \text{IC}_{50}/(1 + [1,8\text{-ANS}]/K_d)$ , where [1,8-ANS] means the concentration of  
35  
36 1,8-ANS used in the assay and  $K_d$  means the dissociating constant for 1,8-ANS with  
37  
38 FABP4 or FABP3. The  $K_d$  values of 1,8-ANS with FABP3, FABP4 or FABP5 were  
39  
40 measured by monitoring the maximal fluorescence signal of 1  $\mu\text{M}$  1,8-ANS with  
41  
42 increasing protein concentrations ranging from 100 nM to 140  $\mu\text{M}$ , and the determined  
43  
44 value is  $11.7 \pm 0.4\text{ }\mu\text{M}$ ,  $2.4 \pm 0.0\text{ }\mu\text{M}$  and  $10.7 \pm 0.6\text{ }\mu\text{M}$ , respectively, using the non-  
45  
46 linear regression in GraphPad Prism software.<sup>45</sup> Three independent experiments were  
47  
48 performed to determine these  $K_d$  values.

49  
50 **ITC Measurements.** All measurements were performed in an ITC buffer (20 mM  
51  
52 HEPES, pH 7.5, 150 mM NaCl) by the iTC200 calorimeter (General Electric Co.). The  
53  
54 compounds were diluted in the ITC buffer to final concentrations of 0.2-0.5 mM. The  
55  
56 purified apo FABP4 was diluted in the ITC buffer to final concentrations of 0.02-0.05  
57  
58 mM. The final concentration of DMSO in a reaction is less than 3%. All titrations were  
59  
60 performed using an initial injection of 0.4  $\mu\text{L}$  followed by 19 identical injections of 2

1  
2  
3  
4  $\mu\text{L}$  with a duration of 4 s per injection and a spacing of 120 s between injections. The  
5 last eight data were averaged as the heat of dilution and subtracted from each titration.  
6  
7 Three independent experiments were carried out to obtain the  $K_d$  value of each  
8 compound with apo FABP4.  
9  
10

11 **MD Simulations.** The crystal structure of FABP4 in complex with fragment **1** in  
12 Pose 1 was used for MD simulations. The protein model was prepared in Schrödinger  
13 suite with the OPLS3 force field.<sup>46</sup> Hydrogen atoms were added to the protein using the  
14 PROPKA tool implemented in Schrödinger suite. The structure of fragment **1** was  
15 optimized using Gaussian 09 program<sup>47</sup> at the B3LYP/6-31G\* level before assigning  
16 its atomic charges and atom types with Antechamber implemented in Ambertools14.<sup>48</sup>  
17 The Amber ff14SB<sup>49</sup> and general Amber force field (GAFF)<sup>50</sup> were applied to FABP4  
18 and fragment **1**, respectively. Sodium ions were added to neutralize the system. The  
19 complex structure was then solvated in a rectangular box of TIP3P water molecules  
20 with  $\sim 8$  Å between the box edge and the protein. The system was first minimized and  
21 then equilibrated using Amber14 in the NPT ensemble at 300 K and 1 bar, and the  
22 harmonic-position restraints were applied to the heavy atoms of FABP4 as well as  
23 fragment **1**. These restraints were tapered off gradually over the equilibration process.  
24 Periodic boundary conditions were applied to the simulation system. Bonds containing  
25 hydrogen atoms were restrained with the SHAKE algorithm to allow an integration  
26 time step of 2 fs.<sup>51</sup> Electrostatic interactions were calculated using the particle-mesh  
27 Ewald (PME) summation algorithm.<sup>52,53</sup> In the production run, the Langevin thermostat  
28 and the Monte Carlo barostat were used to maintain a constant temperature of 300 K  
29 and a constant pressure of 1 bar, respectively. Finally, a 600-ns production run was  
30 resulted.  
31  
32  
33  
34  
35  
36  
37  
38  
39  
40  
41  
42  
43  
44  
45  
46  
47  
48  
49

50 **MD Trajectories Analysis.** Trajectories were converted into formats compatible  
51 with Gromacs v5.1.2 and then analyzed using tools implemented in Gromacs.<sup>48,54</sup> The  
52 root-mean-square deviations (RMSDs) between the simulated and poses of **1** revealed  
53 by crystal structures were calculated using gmx rms tool after an alignment of heavy  
54  
55  
56  
57  
58  
59  
60

atoms of FABP4. Conformations of **1** resulted from the MD simulations were clustered using the gmx cluster tool with the GROMOS algorithm and a RMSD cutoff of 0.3 nm.

**Metabolic Stability in Liver Microsomes.** Microsomes in 0.1 M Tris buffer at pH 7.4 (a final concentration of 0.33 mg/mL), co-factor MgCl<sub>2</sub> (a final concentration of 5 mM), tested compounds (a final concentration of 0.1 μM), co-solvent (0.01% DMSO), and 0.005% bovine serum albumin were incubated at 37 °C for 10 min. The reaction was started by the addition of NADPH (a final concentration of 1 mM). Aliquots were sampled at 0, 7, 17, 30, and 60 min, respectively, and methanol (cold in 4 °C) was added to terminate the reaction. Samples were then analyzed by the liquid chromatography-mass spectrometry (LC-MS)/MS.

**Caco-2 Permeability Assay.** The Caco-2 monolayer assays were conducted according to the standard procedure as previously reported.<sup>55</sup> Briefly, the transport of compounds from the apical side to the basolateral side (A–B) and from the opposite direction (B–A) were measured under the same conditions simultaneously. Propranolol and nadolol were used as the controls of hypertonic and hypotonic, respectively. Digoxin was used as a positive control for P-gp mediated drug efflux. The compound was diluted and added to the appropriate well (pH 6.8 for the apical side and pH 7.4 for the basolateral side) after washing the monolayer three times with Hanks' Balanced Salt Solution (HBSS, Sigma-Aldrich). After incubating the plates at 37 °C for 95 min, samples were collected from the donor side at 5 min and 95 min and from the receiver side at 35 min and 95 min. The concentration of samples was determined by the (LC-MS)/MS.

***In vivo* PK Study of Compound 17 in ICR mice.** Nine ICR male mice, weighting 18–22 g each, were randomly divided into three groups. Compound **17** dissolved in phosphate-buffered saline containing 5% DMSO and 0.5% HPMC was administered orally at a dose 25 mg/kg or 10 mg/kg to two groups of mice. Another group of three mice were injected with a single dose (3 mg/kg) of compound **17** dissolved in DMSO/EtOH/PEG300/NaCl (5/5/40/50, v/v/v/v). Blood samples at seven time points

1  
2  
3  
4 (0.25, 0.5, 1.0, 2.0, 4.0, 8.0, and 24 h) were collected. Plasma concentrations of  
5 compound **17** were analyzed using the LC-MS/MS (Agilent 1260 Infinity LC system  
6 and Agilent 6460 Triple Quad Mass Spectrometer System).  
7  
8

9  
10 **Cell Culture and Differentiation.** Human monocytic leukemia THP-1 cells and  
11 3T3-L1 pre-adipocytes were purchased from American Type Culture Collection  
12 (ATCC, Manassas, USA) and maintained in a humid incubator with 5% CO<sub>2</sub> at 37 °C.  
13 THP-1 monocytes were cultured in ATCC formulated RPMI-1640 medium  
14 supplemented with fetal bovine serum (FBS; Invitrogen, UK) and 0.05 mM 2-  
15 mercaptoethanol. THP-1 monocytes were seeded on 96-well plates at a density of 5 ×  
16 10<sup>4</sup> cells/well and simultaneously incubated with 100 nM phorbol 12-myristate 13-  
17 acetate (PMA; Sigma-Aldrich, St Louis, USA) for 24 h, then suspended THP-1  
18 monocytes were differentiated into adherent THP-1 macrophages. 3T3-L1 pre-  
19 adipocytes were cultured in H-DMEM (Gibco) plus 10% new-born calf serum (NCS;  
20 Invitrogen, UK) and differentiated into mature adipocytes as previously described.<sup>32</sup>  
21 Briefly, cells were stimulated with 0.5 mmol/L 3-isobutyl-1-methylxanthine, 1 μmol/L  
22 dexamethasone and 5 μg/mL insulin in H-DMEM plus 10% FBS two days after  
23 confluence. 48 h later, cells were switched to a differentiation medium (H-DMEM plus  
24 10% FBS and 5 μg/mL insulin). Thereafter, cells were switched into a medium (H-  
25 DMEM plus 10% FBS) and the medium was replaced every 2 days until full  
26 differentiation, which are characterized by the increase of cell volume and the  
27 appearance of clusters of fat droplets in cell.  
28  
29  
30  
31  
32  
33  
34  
35  
36  
37  
38  
39  
40  
41  
42  
43  
44

45 **Cell Viability Assay.** THP-1 macrophages or 3T3-L1 pre-adipocytes were  
46 incubated with tested concentrations of compounds for 24 h before addition of the  
47 CCK-8 reagent (Beyotime, Shanghai, China). After incubation for 1 h, absorbance at a  
48 wavelength of 450 nm was measured using the BIO-TEK SYNERGY4 reader.  
49  
50  
51

52 **Lipolysis Assay.** For the forskolin-stimulated lipolysis, fully differentiated 3T3-L1  
53 cells were incubated with compounds at various concentrations for 24 h. Then the cells  
54 were washed twice with Krebs-Ringer HEPES buffer (KRBH) followed by stimulation  
55  
56  
57  
58  
59  
60

1  
2  
3  
4 with 20  $\mu$ M forskolin diluted in KRBH buffer for 2 h. After that, culture supernatants  
5  
6 were collected and assayed for glycerol levels using a free glycerol reagent kit  
7  
8 (Applygen Technologies Inc, China).

9  
10 **MCP-1 and IL-6 Release from THP-1 Macrophages.** After THP-1 cells were  
11  
12 differentiated into macrophages with 100 nM PMA for 24 h, THP-1 macrophages were  
13  
14 washed twice with PBS gently enough to avoid cells shedding from the bottom of the  
15  
16 plate. Then cells were incubated with various concentrations of compounds for 18 h  
17  
18 prior to 100 ng/mL LPS (Sigma-Aldrich, St Louis, USA) stimulation for another 6 h.  
19  
20 Then the supernatants were collected for measurement of the level of MCP-1 and IL-6  
21  
22 using the Human MCP-1 ELISA Kit and the Human IL-6 ELISA Kit (Abcam, UK),  
23  
24 respectively. Cellular proteins were also collected and measured using the BCA Protein  
25  
26 Assay Kit (Beyotime, Shanghai, China) for calibration.

27  
28 **Animal Treatment.** 6-week-old male C57BL/6J mice were purchased from Model  
29  
30 Animal Research Center of Nanjing University and adaptively fed for 1 week in a 12 h  
31  
32 light-dark cycle with free access to water and standard animal chow. Then mice were  
33  
34 grouped randomly (n = 8 for each group) and given BMS309403 (CSN22610,  
35  
36 CSNpharm, Chicago, USA) or compound **17** at a dose of 50 mg/kg by a gavage  
37  
38 administration 1 h before intraperitoneally injected with LPS in normal saline at a dose  
39  
40 of 5 mg/mL. Vehicle group mice received an identical amount of CMC-Na and saline.  
41  
42 5 h later, serum was collected for measurement of the level of MCP-1 and IL-6 using  
43  
44 the Mouse MCP-1 ELISA Kit and the Mouse IL-6 ELISA Kit (Abcam, UK),  
45  
46 respectively. For tissue damage studies, mice were randomly grouped (n = 8) and  
47  
48 intragastrically administrated once a day with BMS309403 (25 mg/kg) or compound  
49  
50 **17** (10, 25 and 50 mg/kg) for 4 days prior to a single intraperitoneal injection of LPS at  
51  
52 a dose of 10 mg/kg. On the 5th day, blood samples and tissue samples were collected  
53  
54 for the following analysis. Serum ALT, AST and BUN levels were assayed with  
55  
56 commercial enzyme assay kits (Jiancheng, Nanjing, China). All animal experiments  
57  
58 were approved by the Institutional Animal Care and Use Committee of Shanghai  
59  
60 Institute of Materia Medica (Accreditation number: 2019-07-XYC-02).

**Histology.** For histology analysis, mice were sacrificed, and liver, kidney, lung, and spleen were separated immediately and fixed in 4% paraformaldehyde for 24 h at room temperature. The fixed tissues were dehydrated by grading ethanol, cleared in xylene and embedded in paraffin blocks. Tissues were cut and stained with hematoxylin and eosin (H&E). The images were made with an ortho optical microscope (Nikon Eclipse E100, Japan).

**Statistical Analysis.** The values of  $K_i$  or  $K_d$  were expressed as mean  $\pm$  SD from three independent experiments and determined via the nonlinear regression analysis using GraphPad Prism software 8.0 (GraphPad Software, Inc., San Diego, CA, USA). Pharmacological data were represented as mean  $\pm$  SEM of at least three independent experiments for cellular study and mean  $\pm$  SEM of eight mice per group for animal research. Statistical significance of the differences observed between the LPS and the test-compound-treated groups was assessed by the one-way ANOVA method followed by a post hoc Tukey's test to make multiple comparisons. Calculations were made with GraphPad Prism software 8.0. *P* values less than 0.05 were considered statistically significant.

## ASSOCIATED CONTENT

### Supporting Information

Including supplementary figures of multiple X-ray crystal structures, tables, HPLC spectra, NMR spectra, and MS spectra.

Molecular formula strings and some data (CSV)

### Accession Codes

The atomic coordinates and structure factors have been deposited into the Protein Data Bank with accession codes 6LJW (FABP4-1), 6LJX (FABP4-1), 6LJS (FABP4-3), 6LJT (FABP4-6), 6LJU (FABP4-11), and 6LJV (FABP4-17). Authors will release the atomic coordinates and experimental data upon article publication.

## AUTHOR INFORMATION

## Corresponding Authors

For Y.X.: phone, +86-21-50801267; E-mail, [ycxu@simm.ac.cn](mailto:ycxu@simm.ac.cn);

## Author Contributions

#These authors contributed equally. The manuscript was written through contributions of all authors. All authors have given approval to the final version of the manuscript.

## Notes

The authors declare no competing financial interest.

## ACKNOWLEDGEMENTS

This study was supported by the National Key R&D Program of China (No. 2017YFB0202604), the National Natural Science Foundation of China (81661148046, 21877122 and 21807104), and the National Science & Technology Major Project “Key New Drug Creation and Manufacturing Program” of China (Grant No. 2018ZX09711002).

## ABBREVIATIONS USED

FABP, Fatty-acid binding protein; FAs, fatty Acids; ITC, isothermal titration calorimetry; Chloroform-*d*, deuterated chloroform; DMSO-*d*<sub>6</sub>, dimethyl sulfoxide-*d*<sub>6</sub>; dichloromethane, DCM; EtOAc, ethyl acetate; PE, petroleum ether; DMF, *N,N*-dimethylformamide; MeOH, methanol; THF, tetrahydrofuran; EtOH, ethanol; DMSO, dimethyl sulfoxide; AcOH, acetic acid; MeCN, acetonitrile; TEA, triethylamine; BINAP, 2,2'-Bis(diphenylphosphino)-1,1'-binaphthalene; RT, retention time.

## REFERENCES

- (1) Furuhashi, M.; Hotamisligil, G. S. Fatty Acid-Binding Proteins: Role in Metabolic Diseases and Potential as Drug Targets. *Nat. Rev. Drug. Discov.* **2008**, *7*, 489–503.
- (2) Kazemi, M. R.; McDonald, C. M.; Shigenaga, J. K.; Grunfeld, C.; Feingold, K. R. Adipocyte Fatty Acid-Binding Protein Expression and Lipid Accumulation are

1  
2  
3  
4 Increased during Activation of Murine Macrophages by Loll-like Receptor Agonists.  
5 *Arterioscl. Throm. Vas.* **2005**, *25*, 1220–1224.

6  
7 (3) Boord, J. B.; Maeda, K.; Makowski, L.; Babaev, V. R.; Fazio, S.; Linton, M. F.;  
8 Hotamisligil, G. S. Combined Adipocyte-Macrophage Fatty Acid-Binding Protein  
9 Deficiency Improves Metabolism, Atherosclerosis, and Survival in Apolipoprotein E-  
10 Deficient Mice. *Circulation* **2004**, *110*, 1492–1498.

11  
12 (4) Hui, X.; Li, H.; Zhou, Z.; Lam, K. S.; Xiao, Y.; Wu, D.; Ding, K.; Wang, Y.;  
13 Vanhoutte, P. M.; Xu, A. Adipocyte Fatty Acid-Binding Protein Modulates  
14 Inflammatory Responses in Macrophages through a Positive Feedback Loop Involving  
15 c-Jun NH2-Terminal Kinases and Activator Protein-1. *J. Biol. Chem.* **2010**, *285*,  
16 10273–10280.

17  
18 (5) Hotamisligil, G. S.; Bernlohr, D. A. Metabolic Functions of FABPs Mechanisms  
19 and Therapeutic Implications. *Nat. Rev. Endocrinol.* **2015**, *11*, 592–605.

20  
21 (6) Zimmer, J. S.; Dyckes, D. F.; Bernlohr, D. A.; Murphy, R. C. Fatty Acid Binding  
22 Proteins Stabilize Leukotriene A4: Competition with Arachidonic Acid but not Other  
23 Lipoygenase Products. *J. Lipid. Res.* **2004**, *45*, 2138–2144.

24  
25 (7) Makowski, L.; Brittingham, K. C.; Reynolds, J. M.; Suttles, J.; Hotamisligil, G. S.  
26 The Fatty Acid-Binding Protein, AP2, Coordinates Macrophage Cholesterol  
27 Trafficking and Inflammatory Activity. Macrophage Expression of AP2 Impacts  
28 Peroxisome Proliferator-Activated Receptor Gamma and IkappaB Kinase Activities. *J.*  
29 *Biol. Chem.* **2005**, *280*, 12888–12895.

30  
31 (8) Furuhashi, M.; Tuncman, G.; Gorgun, C. Z.; Makowski, L.; Atsumi, G.;  
32 Vaillancourt, E.; Kono, K.; Babaev, V. R.; Fazio, S.; Linton, M. F.; Sulsky, R.; Robl,  
33 J. A.; Parker, R. A.; Hotamisligil, G. S. Treatment of Diabetes and Atherosclerosis by  
34 Inhibiting Fatty-Acid-Binding Protein AP2. *Nature* **2007**, *447*, 959–965.

35  
36 (9) Hotamisligil, G. S.; Johnson, R. S.; Distel, R. J.; Ellis, R.; Papaioannou, V. E.;  
37 Spiegelman, B. M. Uncoupling of Obesity from Insulin Resistance through a Targeted  
38 Mutation in AP2, the Adipocyte Fatty Acid Binding Protein. *Science* **1996**, *274*,  
39 1377–1379.

- 1  
2  
3  
4 (10) Makowski, L.; Boord, J. B.; Maeda, K.; Babaev, V. R.; Uysal, K. T.; Morgan, M.  
5 A.; Parker, R. A.; Suttles, J.; Fazio, S.; Hotamisligil, G. S.; Linton, M. F. Lack of  
6 Macrophage Fatty-Acid-Binding Protein AP2 Protects Mice Deficient in  
7 Apolipoprotein E against Atherosclerosis. *Nat. Med.* **2001**, *7*, 699–705.
- 8  
9  
10  
11 (11) Peeters, W.; de Kleijn, D. P.; Vink, A.; van de Weg, S.; Schoneveld, A. H.; Sze,  
12 S. K.; van der Spek, P. J.; de Vries, J. P.; Moll, F. L.; Pasterkamp, G. Adipocyte Fatty  
13 Acid Binding Protein in Atherosclerotic Plaques is Associated with Local Vulnerability  
14 and is Predictive for the Occurrence of Adverse Cardiovascular Events. *Eur. Heart. J.*  
15 **2011**, *32*, 1758–1768.
- 16  
17  
18  
19 (12) Qiao, Y.; Liu, L.; Yin, L.; Xu, L.; Tang, Z.; Qi, Y.; Mao, Z.; Zhao, Y.; Ma, X.;  
20 Peng, J. FABP4 Contributes to Renal Interstitial Fibrosis via Mediating Inflammation  
21 and Lipid Metabolism. *Cell. Death. Dis.* **2019**, *10*, No. 382.
- 22  
23  
24  
25 (13) Hoo, R. L.; Lee, I. P.; Zhou, M.; Wong, J. Y.; Hui, X.; Xu, A.; Lam, K. S.  
26 Pharmacological Inhibition of Adipocyte Fatty Acid Binding Protein Alleviates both  
27 Acute Liver Injury and non-Alcoholic Steatohepatitis in Mice. *J. Hepatol.* **2013**, *58*,  
28 358–364.
- 29  
30  
31  
32 (14) Hu, B.; Guo, Y.; Garbacz, W. G.; Jiang, M.; Xu, M.; Huang, H.; Tsung, A.; Billiar,  
33 T. R.; Ramakrishnan, S. K.; Shah, Y. M.; Lam, K. S.; Huang, M.; Xie, W. Fatty Acid  
34 Binding Protein-4 (FABP4) is a Hypoxia Inducible Gene that Sensitizes Mice to Liver  
35 Ischemia/Reperfusion Injury. *J. Hepatol.* **2015**, *63*, 855–862.
- 36  
37  
38  
39 (15) Gong, Y.; Yu, Z.; Gao, Y.; Deng, L.; Wang, M.; Chen, Y.; Li, J.; Cheng, B. FABP4  
40 Inhibitors Suppress Inflammation and Oxidative Stress in Murine and Cell Models of  
41 Acute Lung Injury. *Biochem. Biophys. Res. Commun.* **2018**, *496*, 1115–1121.
- 42  
43  
44  
45 (16) Floresta, G.; Pistara, V.; Amata, E.; Dichiara, M.; Marrazzo, A.; Prezzavento, O.;  
46 Rescifina, A. Adipocyte Fatty Acid Binding Protein 4 (FABP4) Inhibitors. A  
47 Comprehensive Systematic Review. *Eur. J. Med. Chem.* **2017**, *138*, 854–873.
- 48  
49  
50  
51 (17) Binas, B.; Danneberg, H.; McWhir, J.; Mullins, L.; Clark, A. J. Requirement for  
52 the Heart-Type Fatty Acid Binding Protein in Cardiac Fatty Acid Utilization. *FASEB*  
53 *J.* **1999**, *13*, 805–812.
- 54  
55  
56  
57  
58  
59  
60

- 1  
2  
3  
4 (18) Maeda, K.; Uysal, K. T.; Makowski, L.; Gorgun, C. Z.; Atsumi, G.; Parker, R. A.;  
5  
6 Bruning, J.; Hertzfel, A. V.; Bernlohr, D. A.; Hotamisligil, G. S. Role of the Fatty Acid  
7  
8 Binding Protein Mal1 in Obesity and Insulin Resistance. *Diabetes* **2003**, *52*, 300–307.
- 9  
10 (19) Hao, J.; Zhang, Y.; Yan, X.; Yan, F.; Sun, Y.; Zeng, J.; Waigel, S.; Yin, Y.; Fraig,  
11  
12 M. M.; Egilmez, N. K.; Suttles, J.; Kong, M.; Liu, S.; Cleary, M. P.; Sauter, E.; Li, B.  
13  
14 Circulating Adipose Fatty Acid Binding Protein is a New Link Underlying Obesity-  
15  
16 Associated Breast/Mammary Tumor Development. *Cell. Metab.* **2018**, *28*, 689–705
- 17  
18 (20) Sulsky, R.; Magnin, D. R.; Huang, Y.; Simpkins, L.; Taunk, P.; Patel, M.; Zhu, Y.;  
19  
20 Stouch, T. R.; Bassolino-Klimas, D.; Parker, R.; Harrity, T.; Stoffel, R.; Taylor, D. S.;  
21  
22 Lavoie, T. B.; Kish, K.; Jacobson, B. L.; Sheriff, S.; Adam, L. P.; Ewing, W. R.; Robl,  
23  
24 J. A. Potent and Selective Biphenyl Azole Inhibitors of Adipocyte Fatty Acid Binding  
25  
26 Protein (aFABP). *Bioorg. Med. Chem. Lett.* **2007**, *17*, 3511–3515.
- 27  
28 (21) Lehmann, F.; Haile, S.; Axen, E.; Medina, C.; Uppenberg, J.; Svensson, S.;  
29  
30 Lundback, T.; Rondahl, L.; Barf, T. Discovery of Inhibitors of Human Adipocyte Fatty  
31  
32 Acid-Binding Protein, a Potential Type 2 Diabetes Target. *Bioorg. Med. Chem. Lett.*  
33  
34 **2004**, *14*, 4445–4448.
- 35  
36 (22) Barf, T.; Lehmann, F.; Hammer, K.; Haile, S.; Axen, E.; Medina, C.; Uppenberg,  
37  
38 J.; Svensson, S.; Rondahl, L.; Lundback, T. N-Benzyl-indolo carboxylic acids: Design  
39  
40 and Synthesis of Potent and Selective Adipocyte Fatty-Acid Binding Protein (A-FABP)  
41  
42 Inhibitors. *Bioorg. Med. Chem. Lett.* **2009**, *19*, 1745–1748.
- 43  
44 (23) Tagami, U.; Takahashi, K.; Igarashi, S.; Ejima, C.; Yoshida, T.; Takeshita, S.;  
45  
46 Miyanaga, W.; Sugiki, M.; Tokumasu, M.; Hatanaka, T.; Kashiwagi, T.; Ishikawa, K.;  
47  
48 Miyano, H.; Mizukoshi, T. Interaction Analysis of FABP4 Inhibitors by X-ray  
49  
50 Crystallography and Fragment Molecular Orbital Analysis. *ACS. Med. Chem. Lett.*  
51  
52 **2016**, *7*, 435–439.
- 53  
54 (24) Xu, Q.; Huang, L.; Liu, J.; Ma, L.; Chen, T.; Chen, J.; Peng, F.; Cao, D.; Yang, Z.;  
55  
56 Qiu, N.; Qiu, J.; Wang, G.; Liang, X.; Peng, A.; Xiang, M.; Wei, Y.; Chen, L. Design,  
57  
58 Synthesis and Biological Evaluation of Thiazole- and Indole-Based Derivatives for the  
59  
60 Treatment of Type II Diabetes. *Eur. J. Med. Chem.* **2012**, *52*, 70–81.

1  
2  
3  
4 (25) Cai, H. Y.; Wang, T.; Zhao, J. C.; Sun, P.; Yan, G. R.; Ding, H. P.; Li, Y. X.;  
5 Wang, H. Y.; Zhu, W. L.; Chen, K. X. Benzbromarone, an Old Uricosuric Drug,  
6 Inhibits Human Fatty Acid Binding Protein 4 *in vitro* and Lowers the Blood Glucose  
7 Level in *db/db* Mice. *Acta. Pharmacol. Sin.* **2013**, *34*, 1397–1402.

8  
9  
10  
11 (26) Cai, H.; Liu, Q.; Gao, D.; Wang, T.; Chen, T.; Yan, G.; Chen, K.; Xu, Y.; Wang,  
12 H.; Li, Y.; Zhu, W. Novel Fatty Acid Binding Protein 4 (FABP4) Inhibitors: Virtual  
13 Screening, Synthesis and Crystal Structure Determination. *Eur. J. Med. Chem.* **2015**,  
14 *90*, 241–250.

15  
16  
17  
18 (27) Hertzfel, A. V.; Hellberg, K.; Reynolds, J. M.; Kruse, A. C.; Juhlmann, B. E.; Smith,  
19 A. J.; Sanders, M. A.; Ohlendorf, D. H.; Suttles, J.; Bernlohr, D. A. Identification and  
20 Characterization of a Small Molecule Inhibitor of Fatty Acid Binding Proteins. *J. Med.*  
21 *Chem.* **2009**, *52*, 6024–6031.

22  
23  
24  
25 (28) Ringom, R.; Axen, E.; Uppenberg, J.; Lundback, T.; Rondahl, L.; Barf, T.  
26 Substituted Benzylamino-6-(trifluoromethyl)pyrimidin-4(1*H*)-ones: a Novel Class of  
27 Selective Human A-FABP Inhibitors. *Bioorg. Med. Chem. Lett.* **2004**, *14*, 4449–4452.

28  
29  
30  
31 (29) Kuhne, H.; Obst-Sander, U.; Kuhn, B.; Conte, A.; Ceccarelli, S. M.; Neidhart, W.;  
32 Rudolph, M. G.; Ottaviani, G.; Gasser, R.; So, S. S.; Li, S.; Zhang, X.; Gao, L.; Myers,  
33 M. Design and Synthesis of Selective, Dual Fatty Acid Binding Protein 4 and 5  
34 Inhibitors. *Bioorg. Med. Chem. Lett.* **2016**, *26*, 5092–5097.

35  
36  
37  
38 (30) Cai, H.; Yan, G.; Zhang, X.; Gorbenko, O.; Wang, H.; Zhu, W. Discovery of  
39 Highly Selective Inhibitors of Human Fatty Acid Binding Protein 4 (FABP4) by Virtual  
40 Screening. *Bioorg. Med. Chem. Lett.* **2010**, *20*, 3675–3679.

41  
42  
43  
44 (31) Lan, H.; Cheng, C. C.; Kowalski, T. J.; Pang, L.; Shan, L.; Chuang, C. C.; Jackson,  
45 J.; Rojas-Triana, A.; Bober, L.; Liu, L.; Voigt, J.; Orth, P.; Yang, X.; Shipps, G. W.,  
46 Jr.; Hedrick, J. A. Small-Molecule Inhibitors of FABP4/5 Ameliorate Dyslipidemia but  
47 not Insulin Resistance in Mice with Diet-Induced Obesity. *J. Lipid. Res.* **2011**, *52*,  
48 646–656.

49  
50  
51  
52 (32) Gao, D. D.; Dou, H. X.; Su, H. X.; Zhang, M. M.; Wang, T.; Liu, Q. F.; Cai, H.  
53 Y.; Ding, H. P.; Yang, Z.; Zhu, W. L.; Xu, Y. C.; Wang, H. Y.; Li, Y. X. From Hit to  
54

1  
2  
3  
4 Lead: Structure-Based Discovery of Naphthalene-1-Sulfonamide Derivatives as Potent  
5 and Selective Inhibitors of Fatty Acid Binding Protein 4. *Eur. J. Med. Chem.* **2018**, *154*,  
6 44–59.

7  
8  
9  
10 (33) Hu, B.; Li, Y.; Gao, L.; Guo, Y.; Zhang, Y.; Chai, X.; Xu, M.; Yan, J.; Lu, P.; Ren,  
11 S.; Zeng, S.; Liu, Y.; Xie, W.; Huang, M. Hepatic Induction of Fatty Acid Binding  
12 Protein 4 Plays a Pathogenic Role in Sepsis in Mice. *Am. J. Pathol.* **2017**, *187*,  
13 1059–1067.

14  
15  
16  
17 (34) Huang, R.; Shi, M.; Guo, F.; Feng, Y.; Feng, Y.; Liu, J.; Li, L.; Liang, Y.; Xiang,  
18 J.; Lei, S.; Ma, L.; Fu, P. Pharmacological Inhibition of Fatty Acid-Binding Protein 4  
19 (FABP4) Protects Against Rhabdomyolysis-Induced Acute Kidney Injury. *Front.*  
20 *Pharmacol.* **2018**, *9*, No. 917.

21  
22  
23  
24 (35) Woolford, A. J.; Day, P. J.; Beneton, V.; Berdini, V.; Coyle, J. E.; Dudit, Y.;  
25 Grondin, P.; Huet, P.; Lee, L. Y.; Manas, E. S.; McMenamain, R. L.; Murray, C. W.;  
26 Page, L. W.; Patel, V. K.; Potvain, F.; Rich, S. J.; Sang, Y.; Somers, D. O.; Trotter, L.;  
27 Wan, Z.; Zhang, X. Fragment-Based Approach to the Development of an Orally  
28 Bioavailable Lactam Inhibitor of Lipoprotein-Associated Phospholipase A2 (Lp-  
29 PLA2). *J. Med. Chem.* **2016**, *59*, 10738–10749.

30  
31  
32  
33 (36) Liu, Q.; Huang, F.; Yuan, X.; Wang, K.; Zou, Y.; Shen, J.; Xu, Y. Structure-Guided  
34 Discovery of Novel, Potent, and Orally Bioavailable Inhibitors of Lipoprotein-  
35 Associated Phospholipase A2. *J. Med. Chem.* **2017**, *60*, 10231–10244.

36  
37  
38  
39 (37) Coe, N. R.; Simpson, M. A.; Bernlohr, D. A. Targeted Disruption of the Adipocyte  
40 Lipid-Binding Protein (AP2 Protein) Gene Impairs Fat Cell Lipolysis and Increases  
41 Cellular Fatty Acid Levels. *J. Lipid. Res.* **1999**, *40*, 967–972.

42  
43  
44  
45 (38) Armstrong, E. H.; Goswami, D.; Griffin, P. R.; Noy, N.; Ortlund, E. A. Structural  
46 Basis for Ligand Regulation of the Fatty Acid-Binding Protein 5, Peroxisome  
47 Proliferator-Activated Receptor Beta/Delta (FABP5-PPARBeta/Delta) Signaling  
48 Pathway. *J. Biol. Chem.* **2014**, *289*, 14941–14954.

49  
50  
51  
52 (39) Wang, Q. S.; Zhang, K. H.; Cui, Y.; Wang, Z. J.; Pan, Q. Y.; Liu, K.; Sun, B.;  
53 Zhou, H.; Li, M. J.; Xu, Q.; Xu, C. Y.; Yu, F.; He, J. H. Upgrade of Macromolecular  
54  
55  
56  
57  
58  
59  
60

1  
2  
3  
4 Crystallography Beamline BL17U1 at SSRF. *Nucl. Sci. Tech.* **2018**, *29*, 681–687.

5 (40) Minor, W.; Cymborowski, M.; Otwinowski, Z.; Chruszcz, M. HKL-3000: the  
6 Integration of Data Reduction and Structure Solution—from Diffraction Images to an  
7 Initial Model in Minutes. *Acta. Crystallogr. D. Biol. Crystallogr.* **2006**, *62*, 859–866.

8 (41) McCoy, A. J.; Grosse-Kunstleve, R. W.; Adams, P. D.; Winn, M. D.; Storoni, L.  
9 C.; Read, R. J. Phaser Crystallographic Software. *J. Appl. Crystallogr.* **2007**, *40*,  
10 658–674.

11 (42) Emsley, P.; Cowtan, K. Coot: Model-Building Tools for Molecular Graphics. *Acta.*  
12 *Crystallogr. D. Biol. Crystallogr.* **2004**, *60*, 2126–2132.

13 (43) Adams, P. D.; Grosse-Kunstleve, R. W.; Hung, L. W.; Ioerger, T. R.; McCoy, A.  
14 J.; Moriarty, N. W.; Read, R. J.; Sacchettini, J. C.; Sauter, N. K.; Terwilliger, T. C.  
15 PHENIX: Building New Software for Automated Crystallographic Structure  
16 Determination. *Acta. Crystallogr. D. Biol. Crystallogr.* **2002**, *58*, 1948–1954.

17 (44) Kurian, E.; Kirk, W. R.; Prendergast, F. G. Affinity of Fatty Acid for rRat Intestinal  
18 Fatty Acid Binding Protein: Further Examination. *Biochemistry* **1996**, *35*, 3865–3874.

19 (45) Jacobs, S.; Chang, K. J.; Cuatrecasas, P. Estimation of Hormone Receptor Affinity  
20 by Competitive Displacement of Labeled Ligand—Effect of Concentration of Receptor  
21 and of Labeled Ligand. *Biochem. Biophys. Res. Co.* **1975**, *66*, 687–692.

22 (46) Harder, E.; Damm, W.; Maple, J.; Wu, C.; Reboul, M.; Xiang, J. Y.; Wang, L.;  
23 Lupyan, D.; Dahlgren, M. K.; Knight, J. L.; Kaus, J. W.; Cerutti, D. S.; Krilov, G.;  
24 Jorgensen, W. L.; Abel, R.; Friesner, R. A. OPLS3: A Force Field Providing Broad  
25 Coverage of Drug-like Small Molecules and Proteins. *J. Chem. Theory. Comput.* **2016**,  
26 *12*, 281–296.

27 (47) Gaussian 09, revision D.01, Frisch, M. J.; Trucks, G. W.; Schlegel, H. B.; Scuseria,  
28 G. E.; Robb, M. A.; Cheeseman, J. R.; Scalmani, G.; Barone, V.; Mennucci, B.;  
29 Petersson, G. A.; Nakatsuji, H.; Caricato, M.; Li, X.; Hratchian, H. P.; Izmaylov, A. F.;  
30 Bloino, J.; Zheng, G.; Sonnenberg, J. L.; Hada, M.; Ehara, M.; Toyota, K.; Fukuda, R.;  
31 Hasegawa, J.; Ishida, M.; Nakajima, T.; Honda, Y.; Kitao, O.; Nakai, H.; Vreven, T.;  
32 Montgomery, Jr. J. A.; Peralta, J. E.; Ogliaro, F.; Bearpark, M.; Heyd, J. J.; Brothers,  
33

1  
2  
3  
4 E.; Kudin, K. N.; Staroverov, V. N.; Keith, T.; Kobayashi, R.; Normand, J.;  
5 Raghavachari, K.; Rendell, A.; Burant, J. C.; Iyengar, S. S.; Tomasi, J.; Cossi, M.; Rega,  
6 N.; Millam, J. M.; Klene, M.; Knox, J. E.; Cross, J. B.; Bakken, V.; Adamo, C.;  
7 Jaramillo, J.; Gomperts, R.; Stratmann, R. E.; Yazyev, O.; Austin, A. J.; Cammi, R.;  
8 Pomelli, C.; Ochterski, J. W.; Martin, R. L.; Morokuma, K.; Zakrzewski, V. G.; Voth,  
9 G. A.; Salvador, P.; Dannenberg, J. J.; Dapprich, S.; Daniels, A. D.; Farkas, O.;  
10 Foresman, J. B.; Ortiz, J. V.; Cioslowski, J.; Fox, D. J. Gaussian, Inc., Wallingford CT,  
11 **2013**.

12  
13  
14  
15  
16  
17  
18  
19 (48) Case, D. A.; Cheatham, T. E., 3rd; Darden, T.; Gohlke, H.; Luo, R.; Merz, K. M.,  
20 Jr.; Onufriev, A.; Simmerling, C.; Wang, B.; Woods, R. J. The Amber Biomolecular  
21 Simulation Programs. *J. Comput. Chem.* **2005**, *26*, 1668–1688.

22  
23  
24  
25 (49) Maier, J. A.; Martinez, C.; Kasavajhala, K.; Wickstrom, L.; Hauser, K. E.;  
26 Simmerling, C. ff14SB: Improving the Accuracy of Protein Side Chain and Backbone  
27 Parameters from ff99SB. *J. Chem. Theory. Comput.* **2015**, *11*, 3696–3713.

28  
29  
30  
31 (50) Wang, J.; Wang, W.; Kollman, P. A.; Case, D. A. Automatic Atom Type and Bond  
32 Type Perception in Molecular Mechanical Calculations. *J. Mol. Graph. Model.* **2006**,  
33 *25*, 247–260.

34  
35  
36  
37 (51) Hess, B.; Bekker, H.; Berendsen, H. J. C.; Fraaije, J. LINCS: A Linear Constraint  
38 Solver for Molecular Simulations. *J. Comput. Chem.* **1997**, *18*, 1463–1472.

39  
40  
41 (52) Darden, T.; York, D.; Pedersen, L. Particle Mesh Ewald - an N.Log(N) Method  
42 for Ewald Sums in Large Systems. *J. Chem. Phys.* **1993**, *98*, 10089–10092.

43  
44  
45 (53) Essmann, U.; Perera, L.; Berkowitz, M. L.; Darden, T.; Lee, H.; Pedersen, L. G. A  
46 Smooth Particle Mesh Ewald Method. *J. Chem. Phys.* **1995**, *103*, 8577–8593.

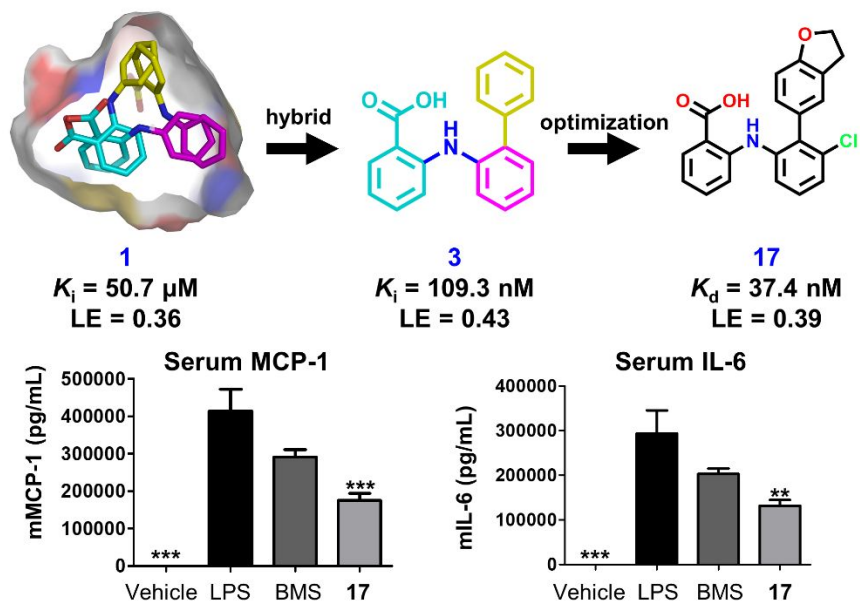
47  
48  
49 (54) Pronk, S.; Pall, S.; Schulz, R.; Larsson, P.; Bjelkmar, P.; Apostolov, R.; Shirts, M.  
50 R.; Smith, J. C.; Kasson, P. M.; van der Spoel, D.; Hess, B.; Lindahl, E. GROMACS  
51 4.5: a High-Throughput and Highly Parallel Open Source Molecular Simulation Toolkit.  
52 *Bioinformatics* **2013**, *29*, 845–854.

53  
54  
55 (55) Skolnik, S.; Lin, X.; Wang, J.; Chen, X. H.; He, T.; Zhang, B. Towards Prediction  
56 of *in vivo* Intestinal Absorption Using a 96-well Caco-2 Assay. *J. Pharm. Sci.* **2010**, *99*,

3246–3265.

1  
2  
3  
4  
5  
6  
7  
8  
9  
10  
11  
12  
13  
14  
15  
16  
17  
18  
19  
20  
21  
22  
23  
24  
25  
26  
27  
28  
29  
30  
31  
32  
33  
34  
35  
36  
37  
38  
39  
40  
41  
42  
43  
44  
45  
46  
47  
48  
49  
50  
51  
52  
53  
54  
55  
56  
57  
58  
59  
60

## Table of Contents Graphic



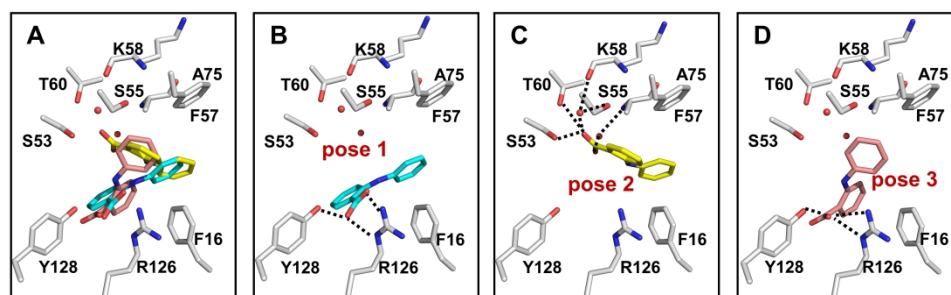


Figure 1. Crystal structures of FABP4 in complex with fragment 1 (PDB codes: 6LJW and 6LJX). (A) An overlay of three binding poses of 1 shown in B-D. (B-D) A representation of three binding poses: Pose 1 (B), Pose 2 (C) and Pose3 (D). Residues interacting with 1 are shown as gray sticks and H-bonds are represented by black dashed lines.

167x55mm (600 x 600 DPI)

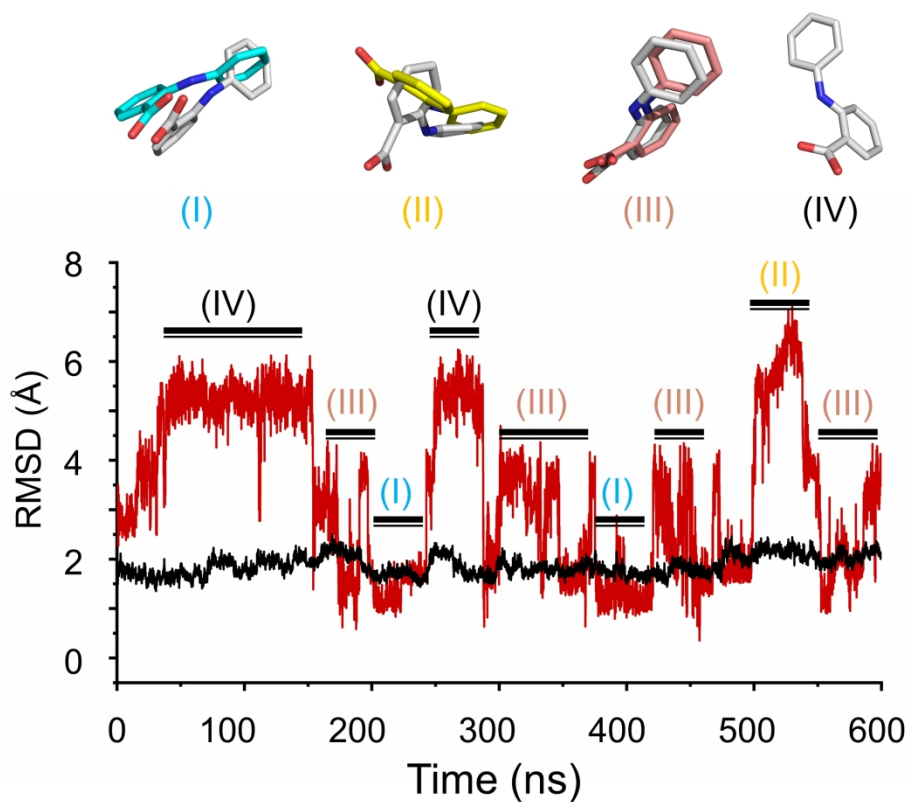


Figure 2. An overlay of representative conformations of fragment 1 extracted from the MD trajectory (gray sticks) with three poses captured by the crystal structures (Pose 1: cyan sticks; Pose 2: yellow sticks; Pose 3: pink sticks). RMSDs of backbone atoms of FABP4 (black) and all atoms of fragment 1 (red) versus the simulation time were calculated based on the MD trajectory of FABP4 in complex with the fragment utilizing Pose 1.

100x83mm (600 x 600 DPI)

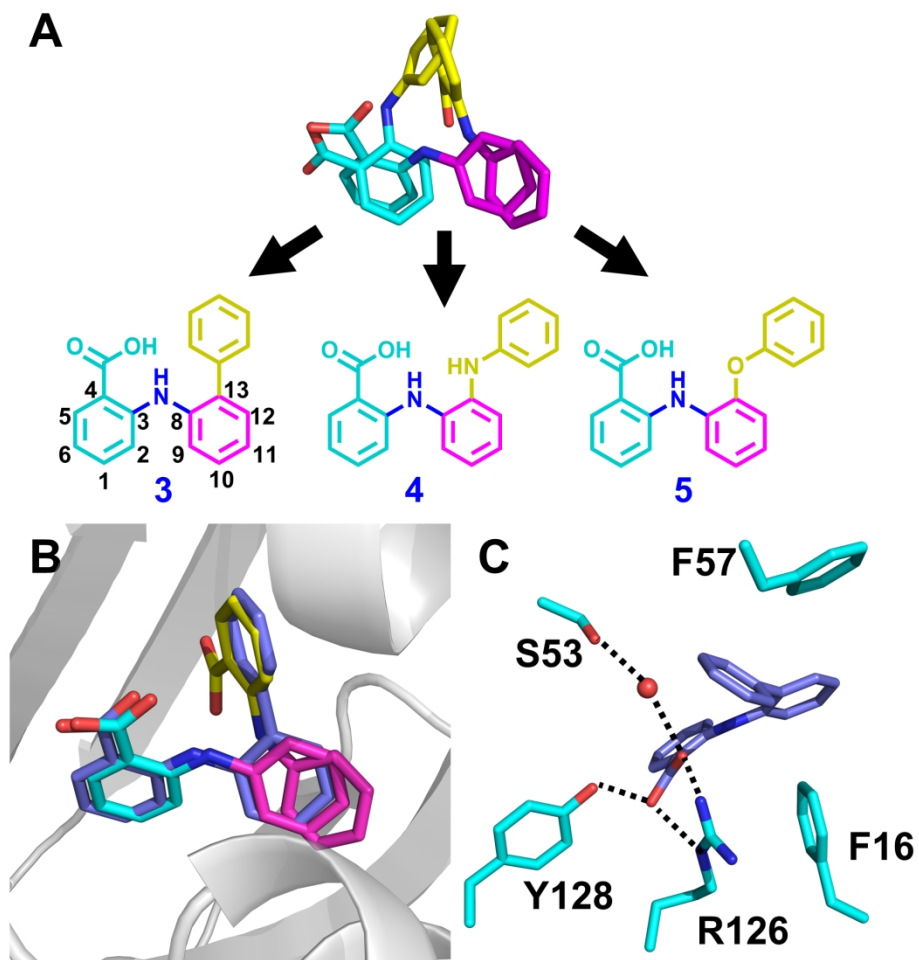


Figure 3. (A) Design of new inhibitors based on different binding poses of fragment 1. (B) An overlay of the binding poses of compound 3 (purple sticks) and fragment 1 by superimposing crystal structures of FABP4 in complex with 3 and 1. (C) Interactions of 3 with the surrounding residues revealed by the crystal structure (PDB code: 6LJS). Residues are shown as cyan sticks and H-bonds are represented by black dashed lines.

90x97mm (600 x 600 DPI)

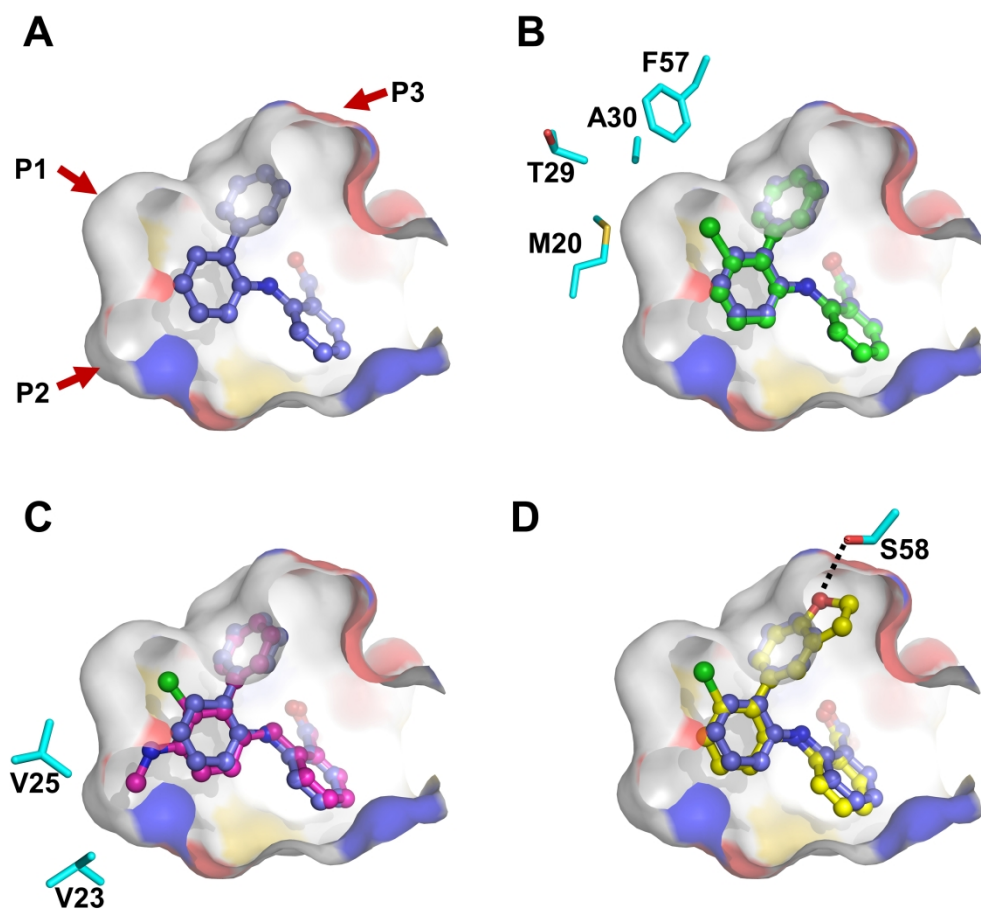


Figure 4. X-ray crystal structures of FABP4 in complex with compounds 3 (purple, A; PDB code: 6LJS), 6 (green, B; PDB code: 6LJT), 11 (magenta, C; PDB code: 6LJU), and 17 (yellow, D; PDB code: 6LJV). Sites P1, P2 and P3 show the optimization directions of compound 3. The ligand binding pocket is presented by molecular surface. The dashed lines indicate H-bonds between compounds and residues.

150x144mm (600 x 600 DPI)

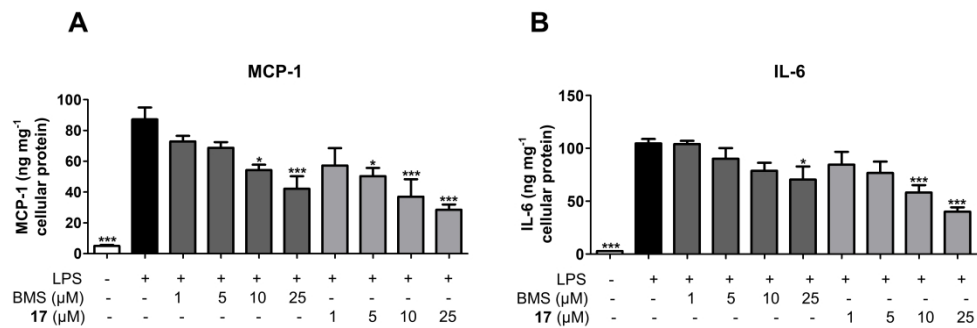


Figure 5. Effects of BMS309403 and compound 17 on the secretion of pro-inflammatory cytokines, MCP-1 (A) and IL-6 (B), in the LPS-induced THP-1 macrophages. MCP-1 and IL-6 were measured by the Elisa Kits. \*P<0.05, \*\*\*P < 0.001 vs LPS group.

178x61mm (600 x 600 DPI)

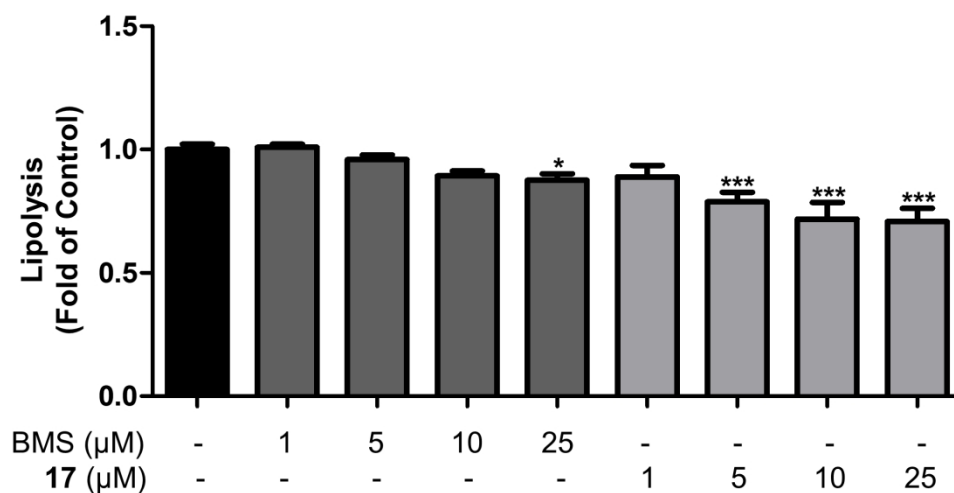


Figure 6. Effect of BMS309403 and compound 17 on the release of free glycerol from the forskolin-stimulated mature 3T3-L1 adipocytes. \*P < 0.05, \*\*\*P < 0.001 vs Control group.

96x55mm (600 x 600 DPI)

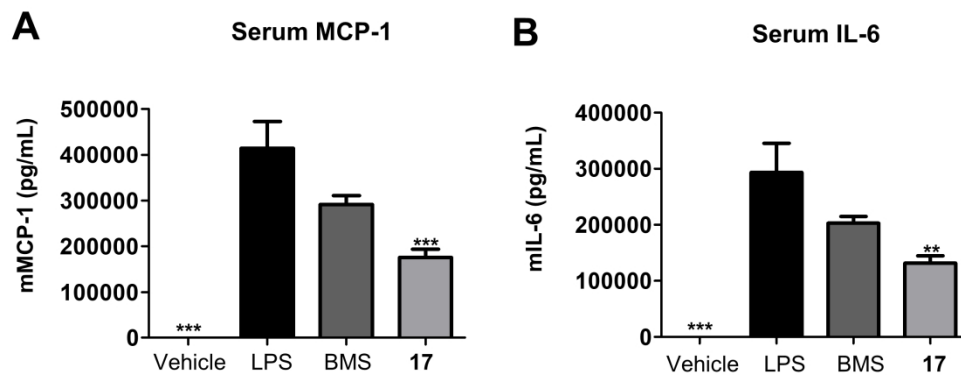


Figure 7. Effects of BMS309403 (50 mg/kg) and compound 17 (50 mg/kg) on the secretion of pro-inflammatory cytokines, MCP-1 (A) and IL-6 (B), in the serum of LPS-treated C57BL/6J mice. MCP-1 and IL-6 were measured by the Elisa Kits. \*\* P < 0.01, \*\*\*P < 0.001 vs LPS group.

128x50mm (600 x 600 DPI)

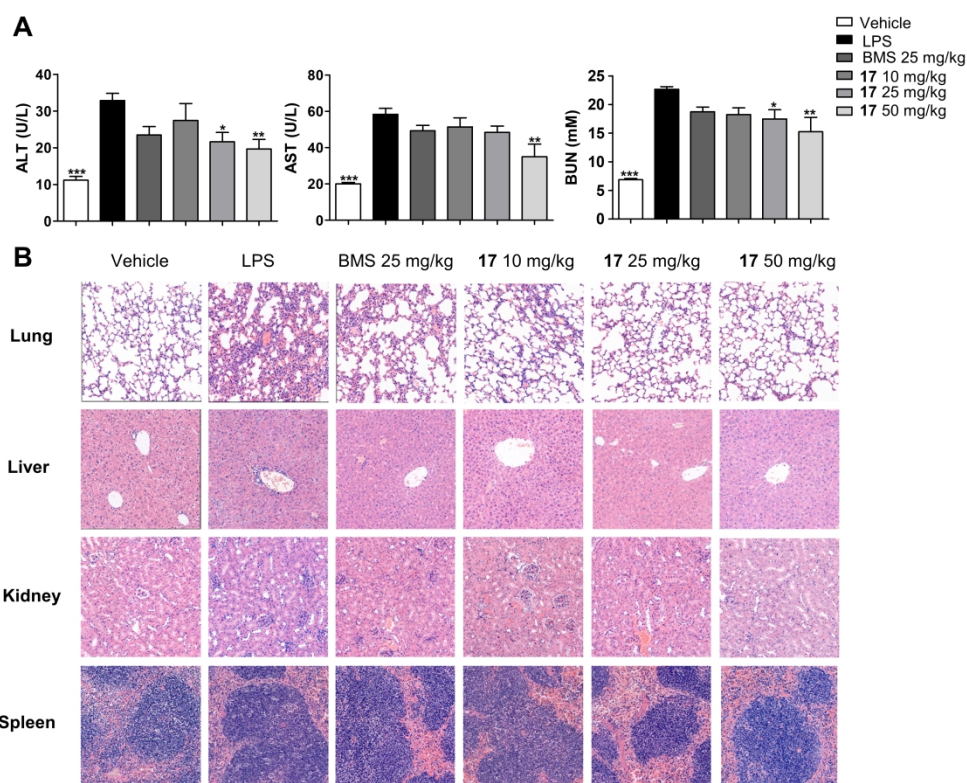
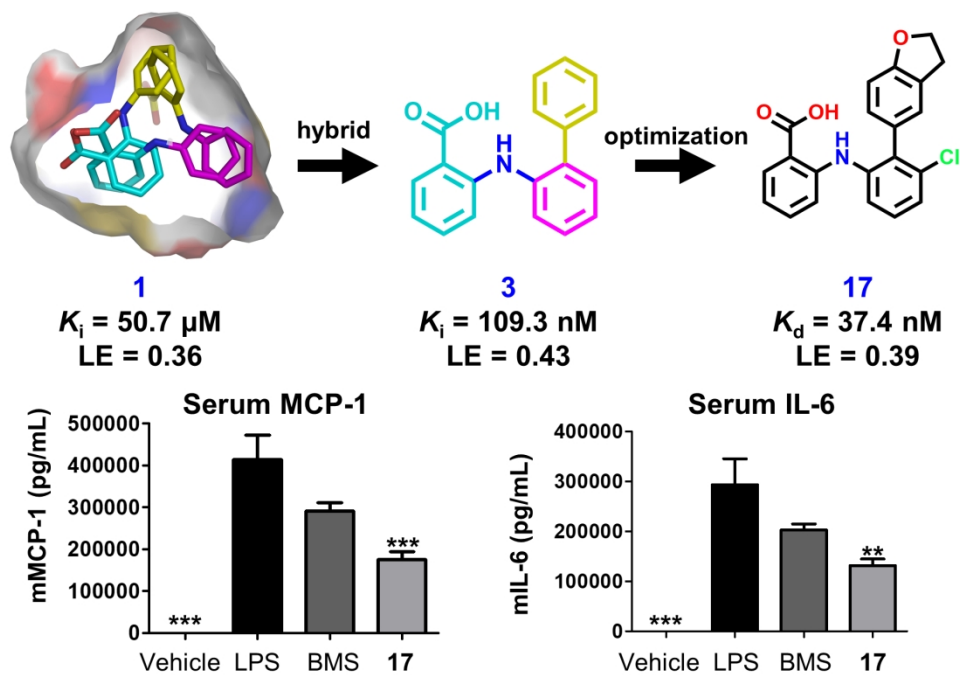


Figure 8. Compound 17 effectively protects mice from the LPS-induced multiorgan damage. (A) BMS309403 (25 mg/kg) or compound 17 (10, 25 and 50 mg/kg) administration decreased the level of tissue damage biomarkers. (B) BMS309403 and compound 17 showed efficient protection against the LPS-induced injury in different organs. (H&E staining, magnification:  $\times 200$ ). Each image is representative of four mice at least. \*  $P < 0.05$ , \*\*  $P < 0.01$ , \*\*\* $P < 0.001$ , each vs LPS group.

180x147mm (600  $\times$  600 DPI)



86x62mm (600 x 600 DPI)